Flow Measurement and Instrumentation 83 (2022) 102107

Contents lists available at ScienceDirect

Flow Measurement and Instrumentation

journal homepage: www.elsevier.com/locate/flowmeasinst

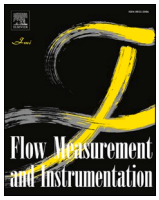

Statistical characterization of the interfacial behavior of the sub-regimes in gas-liquid stratified two-phase flow in a horizontal pipe

Setya Wijayanta [a,b], Indarto [a,c,*], Deendarlianto [a,c], I.G.N.B. Catrawedarma [d], A.Z. Hudaya [e]

[a] Department of Mechanical and Industrial Engineering, Universitas Gadjah Mada, Jalan Grafika No. 2, Yogyakarta, 55281, Indonesia
[b] Study Program of Authomotive Technology, Politeknik Keselamatan Transportasi Jalan, Jalan Semeru No. 3, Kota Tegal, Central Java, 52125, Indonesia
[c] Centre for Energy Studies, Universitas Gadjah Mada, Sekip K-1A, Kampus UGM, Yogyakarta, 55281, Indonesia
[d] Department of Mechanical Engineering, Politeknik Negeri Banyuwangi, Jalan Raya Jember Km. 13, Labanasem, Banyuwangi, 68461, Indonesia
[e] Department of Mechanical Engineering, Universitas Muria Kudus, Kudus, Central Java, Indonesia

ARTICLE INFO

Keywords:
Stratified flow
Power spectral density
Kolmogorov entropy
Discrete wavelet transform

ABSTRACT

The aim of the present study was to identify the interfacial behavior of the sub-regime of gas-liquid stratified two phase flow by using the pressure differential signal data. Here, the probability distribution function (PDF), power spectral density (PSD), kolmogorov entropy and discrete wavelet transform (DWT) were used to analyze the differential pressure signals. The indicators of each flow sub regime were analyzed on the basis of the quantitative values of the statistical curves, which were also validated by visual observation of the video images. The results indicated that there are six identified sub-regimes of stratified flow namely stratified smooth (S), two-dimensional (2-D) wave, three-dimensional (3-D) wave, roll wave (RW), entrained droplet + disturbance wave (ED + DW) and pseudo slug (PS). Next, the increase of liquid viscosity will shift the transition line from the RW to ED + DW to a lower both of J_L and J_G. The increase of the liquid viscosity provides a stabilizing effect to reduce the chaos of the pressure gradient fluctuation. For the RW and the ED + DW sub-regime, the increase of the liquid viscosity shifts the wavelet energy to a larger scale and lower frequency. For the PS sub-regime, the increase of liquid viscosity shifts the wavelet energy to a smaller scale with a higher frequency. For the RW sub-regime, the increase of J_G will increase the wavelet energy at the small-scale and high-frequency decomposition levels.

1. Introduction

Gas-liquid stratified two-phase flow in horizontal pipes is often found in oil and gas transportation systems. The liquid flows along the bottom of the pipe, due to the difference in density between the two phases. The shape of the interface can be smooth or wavy. A good understanding of the interface structure of stratified flow is very important in order to develop the numerical models of adjacent flow regimes such as slug and annular. Therefore, the friction factor of the interface is an important parameter in predicting this transition model [1,2]. Under moderate both gas and liquid flow conditions, the interfacial wave generally has a small amplitude. At higher flow rates, these waves can often grow to large proportions. One example of a large amplitude wave is the roll wave [3]. Under a certain flow condition, the roll wave grows into a slug at the interface through other mechanisms [2]. Slugs with roll waves at lower levels causes the fluctuations of the flow rate and the pressure, whereas it can damage the equipment or instrumentation [4]. On the other hand, high pressure and velocity fluctuations of slug flow in the pipeline causes the pipe to burst/blast [5]. Therefore, slug flow is mostly avoided by engineers and operators in piping systems [6]. Thus, the interfacial structure and the pressure fluctuations in the stratified flow pattern are very important to be studied more deeply, in order to avoid the occurrence of slugs in the piping system. An in-depth understanding of the pressure gradient characteristics enables the industry to obtain the efficient two-phase flow system designs [7].

The interfacial structure of stratified flow has been studied by several researchers using visual methods. Govier and Omer [8]; Mandhane et al. [9]; Taitel and Dukler [1]; divided the stratified flow regime on the basis of the interfacial structure into two sub-regimes, namely stratified smooth and stratified wavy. This category was based on the visual

* Corresponding author. Indarto Department of Mechanical & Industrial Engineering, Faculty of Engineering, Universitas Gadjah Mada, Jalan Grafika No. 2, Yogyakarta, 55281, Indonesia.
E-mail address: indarto@ugm.ac.id (Indarto).

https://doi.org/10.1016/j.flowmeasinst.2021.102107
Received 27 August 2021; Received in revised form 3 December 2021; Accepted 10 December 2021
Available online 10 January 2022

observations of the gas-liquid interface. The stratified smooth flow pattern occurs when both of the superficial gas and liquid velocities are low. When the superficial gas velocity is increased, a wave occurs at the interface resulting in a stratified wavy flow pattern. Spedding and Nguyen [10] conducted a visual study on the two-phase air-water flow regime map and divided the stratified flow into four sub-regimes, namely stratified (smooth), stratified + ripple, stratified + roll wave and stratified + inertial wave. At low water flow rates, the increase of the air flow rate causes a transition from stratified smooth to ripple and then to roll wave. At high air flow rates, the droplets are formed in the water layer. At moderate or nearly full water flow rates, the increase of the air flow rate causes a transition from stratified smooth to inertial wave and then to slug. Chen et al. [11], conducted both experimental and theoretical studies on the air-kerosene stratified wavy flow in a horizontal pipe, and divided the sub-regimes of the stratified flow into:

a. Two-dimensional (2-D) wave flow. Here, the interface is basically flat without any crosswise curvature at the interface.
b. Three-dimensional (3-D) wave flow. Some parts of the liquid phase tend to climb the inner wall of the pipe due to the wave spreading effect, and there is a slight curvature at the interface close to the pipe wall.
c. Roll wave flow. Here, some parts of the liquid phase rise up the inner wall of the pipe and a significant concave down curvature is formed at the air-water interface.
d. Entrained droplet flow. Some parts of the liquid droplets escape from the liquid surface and entrainment/deposition phenomena occur. As the superficial velocity of the gas increases, a significant fraction of the entrainment of the liquid appears in the air stream. It is estimated that an annular flow pattern occurs if the superficial gas velocity is high enough.

Fernandino and Ytrehus [12] conducted an experimental work on the water-air stratified two-phase flow with a rectangular channel section of 7 cm × 7 cm. They divided the stratified flow sub-regimes into stratified smooth, 2-D small amplitude and pebbled, 3-D and large amplitude and large-amplitude waves. Another flow pattern called as the pseudo-slug flow was identified by Lin and Hanratty [2] and Hudaya et al. [13]. Those sub-regimes are distinguished from the slug flow because the liquid slug touches the top of the pipe only momentarily and no blockage occurs. Hudaya et al. [13] distinguished six stratified flow sub-regimes on the basis of the recorded obtained from the experiment images using a high-speed video camera. Those are as smooth, 2-D wave, 3-D wave, roll wave, entrained droplet + disturbance wave and pseudo slug.

From the above reports in the identification of the sub-regime of the stratified flow visually, it shows that the interpretation of video images is subjective, hence the results among the investigators can be different. Therefore, it is necessary to develop a more objective method, whereas, the pressure gradient characteristics of the stratified flow pattern are very important to be studied more deeply in order to obtain an efficient two-phase flow system design. Here, it is necessary to use the pressure differential signal data to identify the stratified flow sub-regime, as well as to obtain the statistical characteristics of them. Several previous researchers have also succeeded in using pressure signal data to identify the flow regimes in a horizontal pipe as seen in Table 1. Although many researchers have identified the flow regime, no one has identified sub-regime on stratified flow using pressure differential signal data.

In addition, other parameters that affect the interface structure/pattern in two-phase flow are the physical properties of the fluid. Andritsos et al. [14] studied the effect of liquid viscosity on the transition from a stratified pattern to a slug pattern in horizontal pipes. They reported that the increase of the liquid viscosity causes a sharp decrease the required superficial fluid velocity for the transition from stratified to intermittent. In addition, Matsubara & Naito [15], also reported that the increase of the liquid viscosity reduces the superficial velocity of the gas at the transition line from the stratified flow to intermittent flow patterns (slug and plug) and the transition from a roll wave to the annular flow.

Table 1
The previous researches of the identification of gas-liquid two phase flow pattern using the pressure sensor in a horizontal pipe.

Authors	Fluids and Regime	Measurement conditions	Method
Cai et al. [26]	Water-air (stratified, slug, intermittent transition and bubble)	Two absolute pressure, D = 50 mm, X_{DP} = 1D, horizontal	Kohonen self-organizing neural network to identify flow regimes
Drahos et al. [27]	Water-air (plug and slug)	Wall pressure fluctuations, D = 50 mm, X_{DP} = 8D, horizontal	Chaotic time series analysis to obtain a new insight into the dynamics of intermittent flow pattern.
Wu et al. [28]	Oil-gas-water (stratified, intermittent and annular)	Differential pressure, D = 40 mm, X_{DP} = 5D, horizontal	The fractal analysis to analyze the signal for identification of flow pattern
Santoso et al. [29]	Water-air (stratified, plug and slug)	Differential pressure, D = 24 mm, X_{DP} = 5D, horizontal	Flow pattern identification method based on PSD and neural network
Saini & Banerjee [30],	Water-air (plug, less aerated slug and highly aerated slug)	Pressure fluctuations, D = 50, 25 and 12 mm, horizontal	Identifying the intermittent flow patterns using the recurrence analysis
Saini & Banerjee [31],	Water-air (stratified, wavy, onset slugging and slug)	Pressure fluctuations, D = 25 mm, horizontal	Recognizing the onset of slug using recurrence analysis (recurrence rate, determinism rate, and entropy)

With the change of the sub-regime in the stratified flow, it is possible to noticed that the instability of the interfacial structure and the pressure fluctuations in transition region between sub-regimes is very likely to occur. Hence, a signal processing is needed to provide the information on the instantaneous state of the flow. In the present study, the differential pressure signal will be analyzed by the Discrete Wavelet Transform (DWT) to explain the stratified flow sub-regime. DWT is a multi-resolution decomposition technique to produce a good local representation signal in both the time and frequency domains simultaneously. DWT provides a signal decomposition time scale which is an intermediary between the time and frequency domains [16]. The special nature of the basic wavelet function makes it possible to obtain a localized distribution of signal energy through the frequency octaves which gives a small dimension of the feature vector. This is very useful, if the Fourier spectrum is relatively featureless, therefore it is able to characterize the flow sub-regime.

The discrete wavelet decomposition for the discrete signal f(t), t = 1,2, …,N can be described as [17].

$$f(t) = \sum_{k\in Z} C_{J_2,k}\varphi_{J_2,k}(t) + \sum_{j=J_1+1}^{J_2}\sum_{k\in Z} D_{j,k}\psi_{j,k}(t) = A_{J_2}f(t) + \sum_{j=J_1+1}^{J_2} D_j f(t) \quad (1)$$

where, $\psi_{j,k}(t)$ is a wavelet function derived by shifting and scaling a function $\psi(t)$ (mother wavelet). $\varphi(t)$ is the scaling function. $A_{J_2}f(t)$ is the approximation signal component on the J_2 scale i.e. the component with a frequency lower than $2^{-J_2}f_{max}$, where f_{max} is the maximum signal frequency that can be measured. $D_j f(t)$ is the signal detail component on the scale $j(J_1 + 1 \le j \le J_2)$, which is a frequency band component with respectively end points located at $2^{-j}f_{max}$ and $2^{-j+1}f_{max}$:

$$D_j f(t) = \sum_{k\in Z} D_{j,k}\psi_{j,k}(t) \quad (2)$$

The coefficients $C_{J_2,k}$ and $D_{j,k}$ in Eqs. (1) and (2) are the wavelet decomposition coefficients, which can be calculated recursively from $C_0(f(t))$ using the Pyramid algorithm. Eq. (1) means that the discrete signal $f(t)$ separates DWT into low frequency components and a series of components in different frequency bands which is called multiresolution analysis. Due to the orthogonality of the wavelet base, the energy of the signal fluctuation can be represented by the decomposition coefficient. The local energy of the signal on the j scale is represented as:

$$E_j = \sum_{k \in Z} D_{j,k}^2 \quad J_1 + 1 \le j \le J_2 \tag{3}$$

The entire-scale energy wavelet distribution can be treated as the decomposition of the signal variance into a scale, therefore the entire-scale energy distribution can be used as an indicator of the sub-regimes.

The aim of the present experimental study is to identify the interfacial behavior of the sub regimes of gas-liquid two-phase stratified flow by using the differential pressure signals. Here, the probability distribution function (PDF), power spectral density function (PSD), kolmogorov entropy and wavelet analysis are used to distinguish each sub-regime in the stratified flow. The indicators of each flow sub regimes were analyzed on the basis of the quantitative values of the statistical curves, which were also validated by visual observation of the captured video images.

2. Experimental apparatus and method

The present experimental study was conducted at the Fluid Mechanics Laboratory, Department of Mechanical and Industrial Engineering, Universitas Gadjah Mada, Indonesia. The working fluids were air and water. To vary the viscosity of the liquid, the water is mixed with the glycerine with the percentage of glycerin in the mixture was 30% and 50% as shown in Table 2. In the present work, the main parameters were the superficial velocity of liquid (J_L) and air (J_G), pressure gradient and sub flow regime. To simplify the explanation in this paper, we have used some abbreviations for the test liquids on the basis of their viscosities. The abbreviations in this paper are as follows: **W**: Air-water (dynamic viscosity μ = 1.002 mPa s), **G30**: Air-30 wt% glycerine (μ = 2.773 mPa s) and **G50**: Air-50 wt% glycerine (μ = 6.292 mPa s).

The schematic diagram of the experimental apparatus used in the present study is shown in Fig. 1. The test section was made of transparent acrylic pipe with an inner diameter of 26 mm and a length of 9.5 m (approximately 365 D). The water from the storage tank (inlet) and air from the compressor tube flow through the flow meter and into the mixer. In the mixer, each inlet was separated by a flat plate to form a stratified flow, then flows through the test section pipe to the separator. Water and air were separated in a separator, where the air was released into the atmosphere, meanwhile the water was collected by the outlet tank to be flowed back to the inlet tank. Here, J_L was set from 0.02 m/s to 0.1 m/s, while J_G was set from 4 m/s to 16 m/s.

The flow characteristics were observed by using the Phantom Miro 310 high speed video camera (HSV) as reported also by Hudaya et al. [13]. In the present study, HSV was set from 120 to 240 fps to capture the stratified flow phenomenon. The test section for visualization was equipped with a correction box made of transparent acrylic sheet placed at a distance of 5 m (192 D) from the inlet, to ensure a fully developed flow. The area between the correction box and the test section was filled with water because the refractive index of acrylic is almost to that of the water, thus reducing visual distortion. The lighting correction box was made up of rows of LED lights and layered, highlighted from behind to get the best picture. The pressure gradient between the two locations (pressure tap) installed on the liquid side of the stratified flow on the test section pipe was measured using a differential pressure transducer (DPT) as shown in Fig. 1. By measuring the pressure difference between two pressure taps, it is expected to get time series signal data for the average pressure drop. From the momentum conservation equation, the pressure drop is strongly influenced by the interfacial shear stress, and the interfacial shear stress is strongly influenced by the interfacial structure of the stratified flow. Therefore, in the present experimental study, time series of the pressure difference signals are used to analyze the interface structure along the test section.

Table 2
Physical properties of the tested liquid.

Liquid	ρ (kg/m^3)	μ (mPa.s)	σ (mN/m)
Water (**W**)	997	1.002	72
Water + Glycerine 30% (**G30**)	1073	2.773	69.2
Water + Glycerine 50% (**G50**)	1100	6.292	68

The equations to calculate the interfacial friction factor (*fi*) has been developed by Andritsos & Hanratty (1987) and Tzotzi & Andritsos (2013) using the liquid film thickness, while Hart et al. (1989) and [11] used the liquid holdup and wetted wall fraction. The interfacial friction factors (*fi*) are used to calculate the interfacial shear stress and predict the pressure drop. From these facts, it is considered that the pressure tap is placed on the liquid side of the stratified flow in the test section pipe to obtain more precise data and analysis. The first pressure tap is placed at a distance of 4400 mm (approximately 169 D) from the inlet, while the distance between the first and second pressure taps is 1600 mm (approximately 61 D). Meanwhile, the downstream pipe is intended for the installation of parallel wire conductance probes to measure liquid film thickness and calculate stratified flow wave parameters. However, it is not included in the present manuscript. The present manuscript focuses on the study of the results of visualization study and statistical characteristics of the interface behavior in the stratified flow using a differential pressure transducer (DPT). Here, the DPT brand Valydine with a capacity of 55 kPa of the accuracy of 0.25% was used. The voltage signal generated by the DPT was amplified by a pressure amplifier, then forwarded to data aquitition (DAQ) and recorded by a computer (PC) with the sampling rate of 1000 data/second.

3. Results and discussions

3.1. Sub regime and the flow pattern maps

In the range of both J_L and J_G of the working fluid of **W** in the present study, there are six identified sub-regimes of the stratified flow as identified also by Hudaya et al. [13]. Those are stratified smooth, two-dimensional (2-D) wave, three-dimensional (3-D) wave, roll wave (RW), entrained droplet and disturbance wave (ED + DW) and pseudo slug (PS). Meanwhile under the condition of the working fluid of **G30** and **G50**, two-dimensional (2-D) wave, three-dimensional (3-D) wave do not appear during the observation as shown clearly in Fig. 2.

Close observation of the flow map as shown in Fig. 2, it is noticed that the increase of the liquid viscosity, the transition line from the RW to ED + DW shifts to the lower both J_L and J_G. In addition, the sub regimes of the 3-D wave and RW at $J_G = 6$ m/s change to PS, while RW at $J_G = 5$ m/s changes to smooth. Next, the 2-D wave sub-regime changes to smooth. Thus, the increase of the liquid viscosity from **W** to **G30** and **G50** decreases the RW region, while it increases the region of the stratified smooth, PS and ED + DW. This is also in a good agreement with that of Matsubara & Naito, [15].

The physical mechanism of the sub-regimes in stratified flow can be seen in Fig. 3, and explained as follows:

– **Transition from smooth to 2D wave**

The small addition of J_G from the stratified smooth causes the growth of 2-D waves. Visually, an example of a transitional physical mechanism from a smooth to 2-D wave sub regime with a tested liquid **W** at J_L = 0.03 m/s and J_G = 5 m/s can be seen in Fig. 3(a). Hanratty (1983) suggested that these 2-D waves are generated by pressure variations and energy transfer from air to liquid through normal velocity fluctuations to

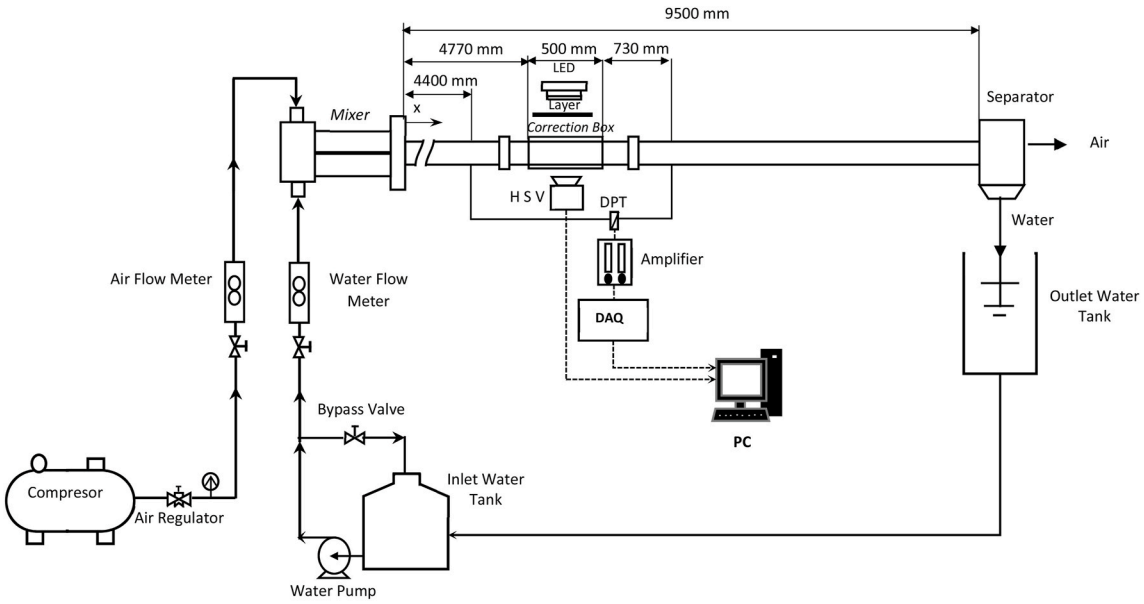

Fig. 1. Experimental apparatus.

the interface. The observations in this study indicate that 2-D waves do not appear continuously, but appear in clusters and maintain their identity over several periods. This is also in accordance with the observation results from Andritsos's (1992).

– **Transition from 2D to 3D wave**

The increase of J_G from the condition of the 2-D wave sub regime causes the growth of 3-D waves with irregular shapes. Visually, an example of a transitional physical mechanism from a sub-regime of 2-D wave to 3-D wave under a tested liquid **W** at $J_L = 0.03$ m/s and $J_G = 6$ m/s can be seen in Fig. 3 (b) [14]. uses a physical interpretation of the Kelvin-Helmholtz (KH) instability to explain the physical mechanism of the growth of 3-D wave. The increase of J_G from the sub regime of the 2-D wave decreases the pressure above the liquid due to the Bernoulli effect. This pressure decrease causes the liquid to be more lifted and increases the destabilization of the interface so that increases the wave amplitude and forms the 3-D waves. The observations in this study indicate that 3-D waves do not appear continuously, but appear in clusters, irregular and maintain their identity over several periods.

– **Transition from 3D to RW**

The increase of J_G from the condition of the sub regime of 3-D wave causes the growth of RW. An example of the transition of the sub-regime 3-D wave to RW with tested liquid **W** at $J_L = 0.03$ m/s and $J_G = 8$ m/s can be seen in Fig. 3 (c). The increase of J_G causes several 3-D waves to be pushed forward and the coalescence a small wave occurs with a larger and higher waveform. The impetus from the air flow continues, so that the crest of the wave will form a roll called a RW. Under this flow condition, RW does not appear continuously, but their appearance is in the clustered form.

– **Transition from RW to ED + DW**

The increase of J_G from the RW sub-regime condition causes the appearance of disturbance wave and entrained droplet. An example of a transition from a sub-regime RW to ED + DW under the tested liquid **W** at $J_L = 0.03$ m/s and $J_G = 16$ m/s can be seen in Fig. 3(d). The increase of J_G from the sub regime of the RW decreases the pressure above the liquid, hence the liquid is lifted from the bottom and forms a thin layer on the pipe wall (disturbance wave). Some of the liquid layer will be released in the form of droplets at the top wall of the pipe, it forms a sub-regime of entrained droplet + disturbance wave (ED + DW). Lin and Hanratty [2] reported that the droplet deposition on the pipe wall is one of the initial mechanisms for the occurrence of the annular flow.

– **Transition from RW to Pseudo slug (PS)**

The increase of J_L and reduction of J_G from the condition of the RW sub regime causes the occurrence of PS. An example of a transition from the sub-regime RW to PS under the tested liquid **W** at $J_L = 0.05$ m/s and $J_G = 5$ m/s can be seen in Fig. 3 (e). Under this flow condition, it causes the increases of the size of the RW and decreases its movement, hence the waves behind it collide with the waves in front of it. This wave coalescence causes a hydraulic jump, in which the liquid briefly touches the top of the pipe and is immediately decayed by the force of the air. This event is called as the pseudo slug, because there is no blockage in the pipe.

– **Transition from smooth to Pseudo slug (PS)**

The increase of the viscosity of the liquid from **W** (1002 mPa s) to **G30** (2773 mPa s) and **G50** (6292 mPa s) caused no 2-D waves in the ranges of J_L and J_G in this experiment. This is due to the low J_G being unable to overcome the viscous dissipation or stabilizing effect by the increase of the liquid viscosity. Meanwhile, the 3-D wave also did not appear and changed to pseudo slug at $J_G = 6$ m/s. An example of the transition from the smooth to PS under **G50** tested liquid at $J_L = 0.03$ m/s and $J_G = 6$ m/s can be seen in Fig. 3(f). The increase of J_G from 5 m/s to 6 m/s forms an aerated bubble on the surface of the liquid. It is getting bigger and bigger until covers the pipe cross section for a moment (pseudo slug) until finally decays and returns to a smooth interface condition.

To describe each sub-regime of the three tested liquids (**W**, **G30** and **G50**), $J_L = 0.02$ m/s was chosen as an example of the stratified smooth sub-regime, while the sample for stratified wavy was selected under the condition of $J_L = 0.03$ m/s, and $J_L = 0.05$ m/s and $J_G = 0.05$ m/s for PS. The examples of each sub-regimes can be seen in Figs. 4–6. The important informations from the figures can be summarized as follows. The stratified smooth flow occurs at low both J_L and J_G. An example can be seen in column (a) of Figs. 4 (i), 5 (i and ii) and 6 (i and ii), in which

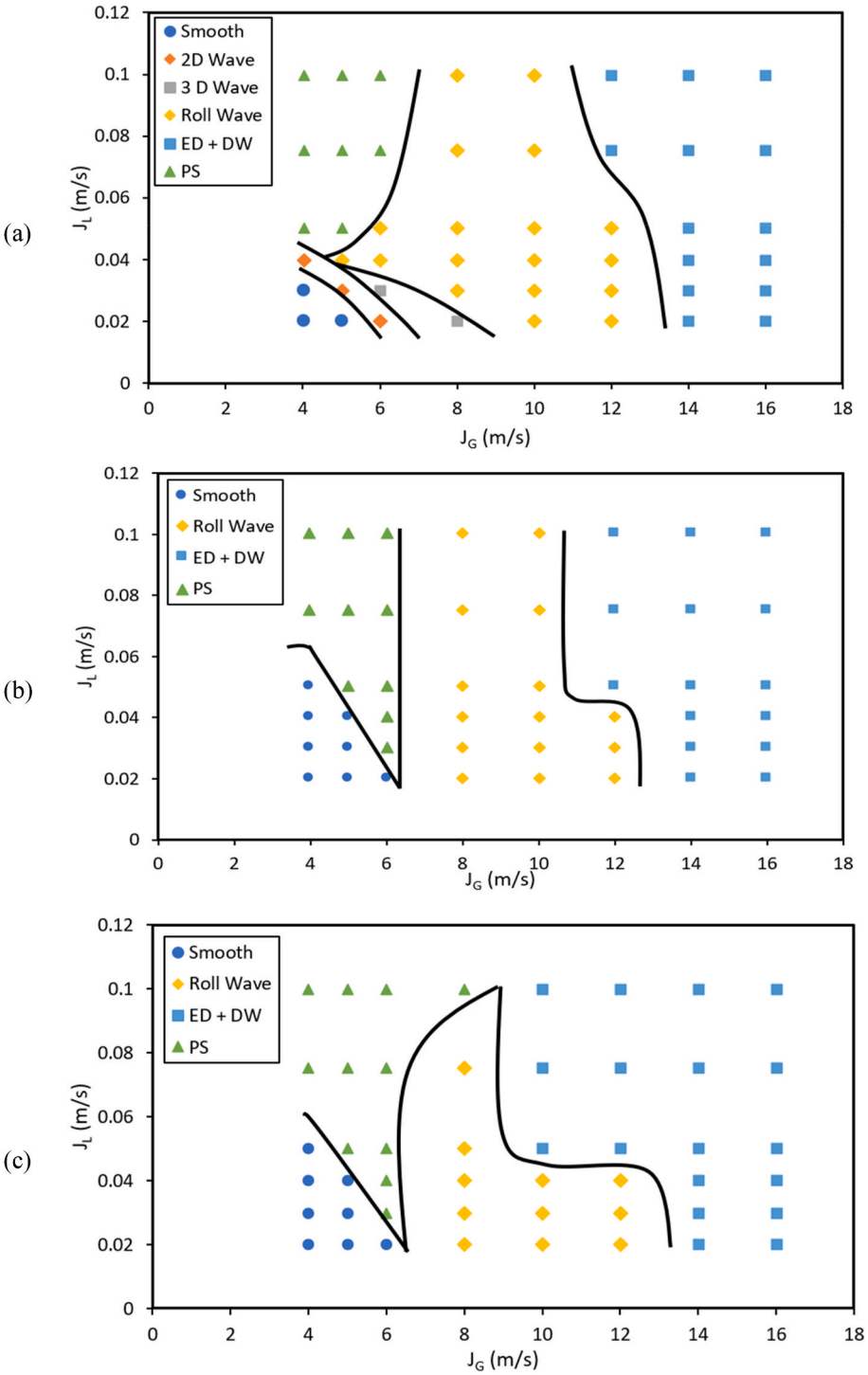

Fig. 2. The map of sub regimes in gas-liquid stratified flow (a) **W**, (b) **G30** and (c) **G50**.

the interface of the liquid and gas phases is flat. In the time series graph, the pressure gradient signal (column b) looks even. In the PDF graph (column c), it can be seen that the pressure gradient fluctuations are very small (<0.1 kPa/m) and the distribution of pressure gradient data appears to be clustered in comparison to that of the other sub-regimes. In the PSD graph (column d), it can be seen that the magnitude of the dominant frequency of the stratified smooth is the lowest value (<1).

In the case of the tested liquid of **W**, the increase of both superficial velocities of gas and liquid from stratified smooth conditions, it causes the formation of the small waves at the liquid and gas interface. These small waves are called 2-D waves. An example of 2-D wave under the flow condition of $J_L = 0.03$ m/s and $J_G = 5$ m/s can be seen in Fig. 4 (ii) column (a). Here, both liquid and gas phases are still completely separated, but small waves appear with a relatively uniform shape. The time series of the pressure gradient signal can be seen in Fig. 4 (ii) column (b), whereas no significant fluctuation in pressure gradient. Meanwhile, from the PSD graph in Fig. 4 (ii) column (d) it can be seen that the dominant frequency is low. This is due to the 2D waves appear discontinuous in clusters with a certain time lag. The magnitude of the dominant frequency is twice as large as that of the stratified smooth. In the experiments by using tested liquids **G30** and **G50**, under the same J_L and J_G, the interface between the liquid and gas phases is still smooth.

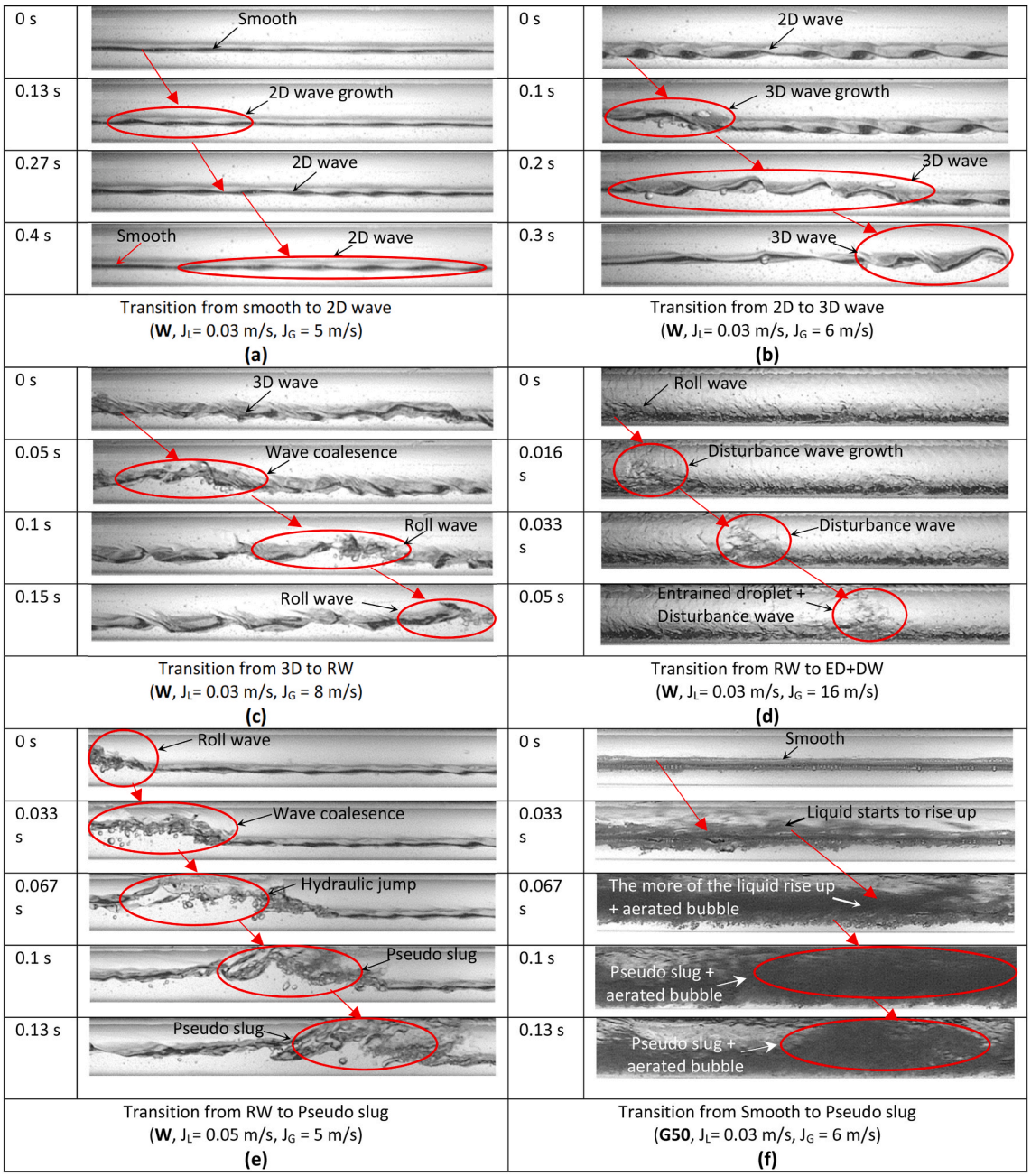

Fig. 3. The physical mechanism of sub-regime transition in stratified flow.

In the case of tested liquid of **W**, the increase of the superficial velocities both of gas and liquid from the 2-D wave causes the formation of 3-D waves. As described by Chen et al., [11]; in the 3-D waves, some parts of the liquid phase tend to climb the inner wall of the pipe due to the wave spreading effect, and there is a slight curvature at the interface close to the pipe wall. Bae et al. [18], reported that the 3-D waves have a regular frequency with the irregular shape in the lateral direction of the flow channel. The example of 3-D wave under the flow condition of J_L = 0.03 m/s and J_G = 6 m/s can be seen in Fig. 4 (iii) column (a). In the figure, the waves are formed with peaks and valleys periodically with irregular shapes in the lateral direction due to the breaking of the waves resulting from the water flowing into the side walls of the pipe. The time series of the pressure gradient signal can be seen in Fig. 4 (iii) column (b), which shows a significant increase in pressure gradient fluctuations in comparison to that of both stratified smooth and 2-D waves. In addition, it can be seen in the PDF in Fig. 4 (iii) column (c), the pressure gradient distribution is wider than the stratified smooth and 2-D wave. From the PSD in Fig. 4 (iii) column (d), it can be seen that the dominant frequency is low, but the magnitude value is approximately six times greater than the 2-D wave at the same J_L.

Under the flow condition of J_L = 0.03 m/s and J_G = 6 m/s of the tested liquids of **G30** and **G50**, the increase of J_G produces a hydraulic jump as a characteristic of PS, as described also by Ref. [2]. The photo of this sub-regime can be seen in column (a) of Fig. 5 (iii) and 6 (iii). A sudden increase in the waves (hydraulic jump) occurs until it reaches the top of the pipe, but the liquid has not completely filled the cross section of the pipe. An increase in J_L but at a lower J_G (J_L = 0.05 m/s and J_G = 5 m/s) causes the occurrence of a larger hydraulic jump in the three liquid fluids (**W**, **G30** and **G50**). The photo can be seen in column (a) in Fig. 4 (vii), 5 (vii) and 6 (vii). This is in accordance with the previous study of Dukler and Hubbard [19], regarding the transition from stratified to intermittent. An example of a time series of the pressure gradient signal

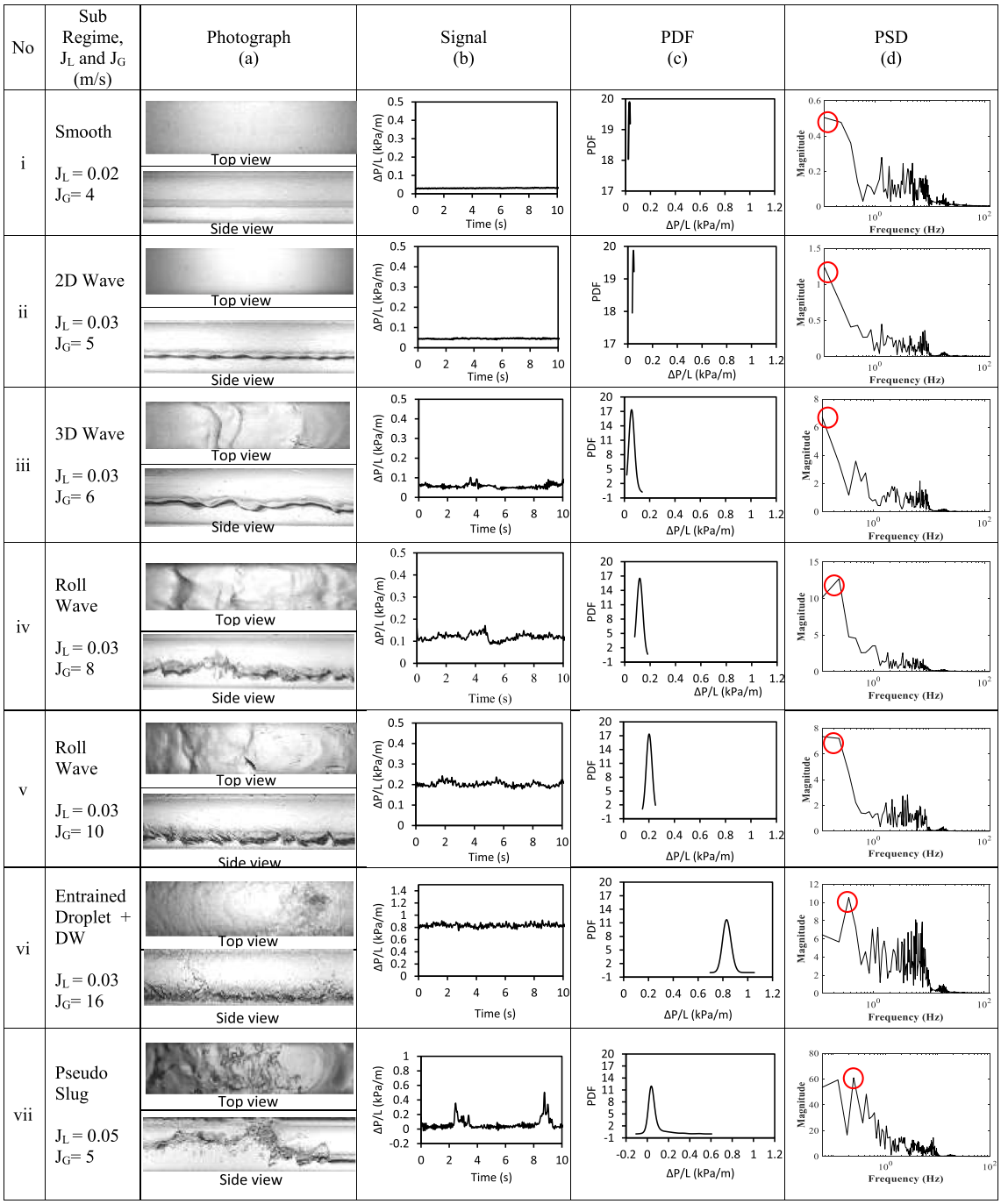

Fig. 4. Example of photos, pressure gradient signal, PDF and PSD of stratified flow regime with liquid fluid (**W**).

can be seen in column (b) in Fig. 4 (vii), 5 (iii), 5 (vii), 6 (iii) and 6 (vii), whereas the fluctuation the pressure gradient appears to be larger than that of the other sub-regimes. In column (c) it can be seen that the PDF has a long tail on the right which indicates that the high-pressure gradients due to hydraulic jumps occur less frequently than low pressure gradients. This can also be seen in the PSD image in column (d) which shows the dominant frequency of the pressure gradient is quite low (<1) but has a very large magnitude.

Under the same $J_L = 0.03$ m/s, the increase of J_G from 6 m/s to 8 m/s and 10 m/s, the gas-liquid interface changes into coils as a feature of the sub regime of RW. It can be seen in column (a) of Fig. 4 (iv and v), 5 (iv and v) and 6 (iv and v). At $J_G = 8$ m/s, the formed RW is larger than that of $J_G = 10$ m/s. This can also be seen from the time series of the pressure gradient fluctuations in columns (b) of Fig. 4 (iv and v), 5 (iv and v) and 6 (iv and v). The fluctuations in RW are larger than that of both 2-D and 3-D waves, but smaller than PS. From the PDF in column (c) of Fig. 4 (iv and v), 5 (iv and v) and 6 (iv and v), it can be seen that the distribution of pressure gradient fluctuations is wider than both 2-D and 3-D waves. In addition, the PSD graphs in column (d) of Fig. 4 (iv and v), 5 (iv and v) and 6 (iv and v) show that the dominant frequency and magnitude of pressure gradient fluctuations are higher than that of both 2-D and 3-D waves. In comparison to the PS, the frequency of the dominant pressure gradient fluctuation is higher, but the magnitude is lower.

Under the same $J_L = 0.03$ m/s, the increase of J_G from 10 m/s to 14 m/s and 16 m/s, it is noticed that the droplets are found at the top wall of the pipe. Here, the liquid is lifted from the bottom of the pipe and begins to form a thin film on the pipe wall. This phenomenon was identified as the occurrence of the ED + DW sub-regime. This droplet

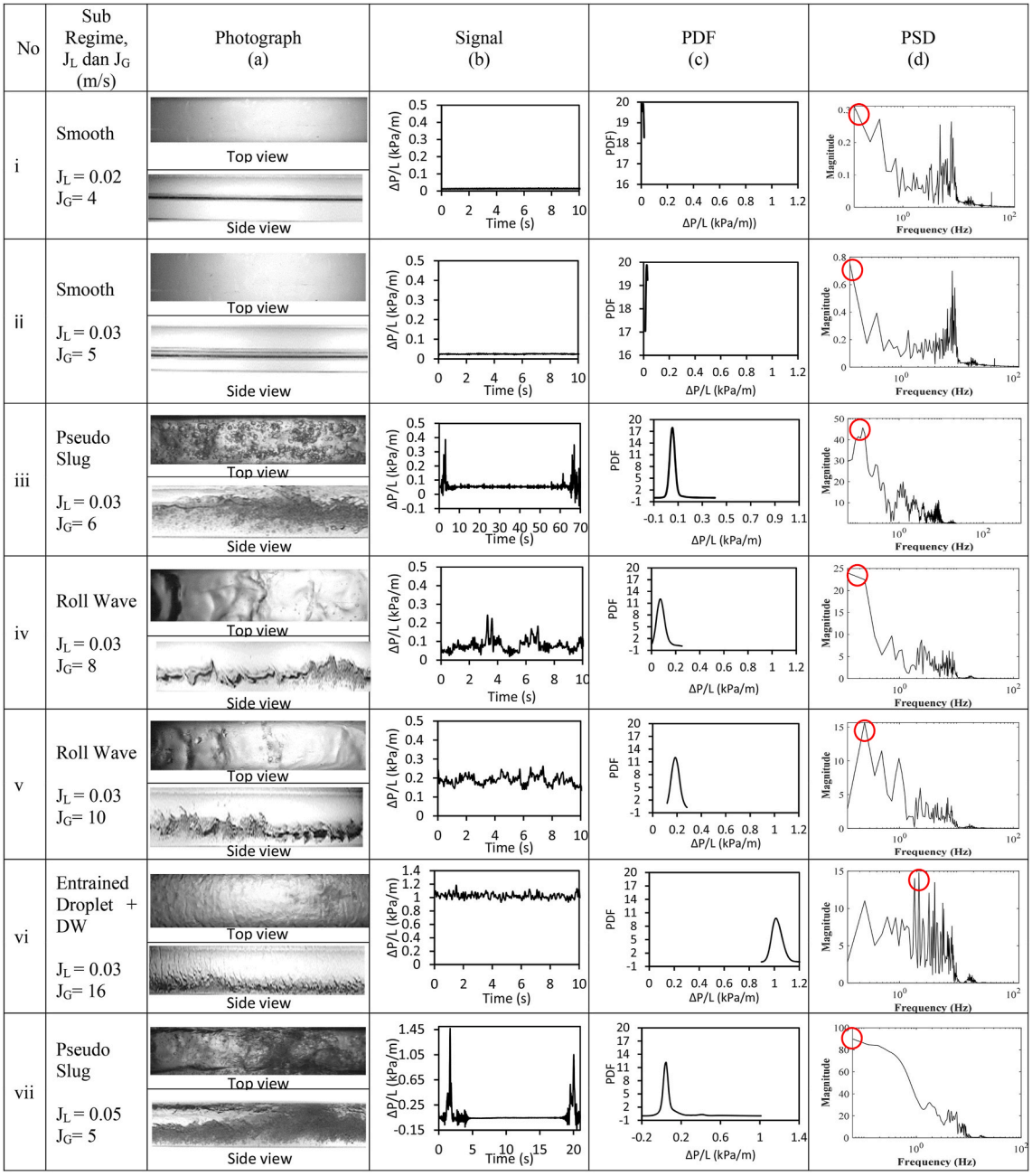

Fig. 5. Example of photos, pressure gradient signal, PDF and PSD of stratified flow regime with liquid fluid (**G30**).

deposition was reported also by Lin and Hanratty [2] as one of the initial mechanisms for the occurrence of annular flow. This is consistent with a study of Dukler and Hubbard [19]; in which at higher gas velocities, the liquid was insufficient to maintain its state and was swept around and up the pipe to form an annulus with some entrainment. These sub-regimes can be seen in column (a) of Fig. 4 (vi), 5 (vi) and 6 (vi). From the time series of the pressure gradient in column (b) of Fig. 4 (vi), 5 (vi) and 6 (vi), it can be seen that the average pressure gradient is higher than the other sub-regimes. However, the amplitude is lower that of RW and PS. From the PDF of the pressure gradient fluctuations in column (c) of Fig. 4 (vi), 5 (vi) and 6 (vi), the distribution of pressure gradient fluctuations looks more spread out than the smooth, 2-D wave, 3-D wave and RW. From the PSD of pressure gradient fluctuations in column (d) of Fig. 4 (vi), 5 (vi) and 6 (vi), the dominant frequency of pressure gradient fluctuations is higher than the other sub-regimes, with a magnitude equal to PS.

3.2. Stochastic analysis

From the pressure gradient signals in column (b) of Figs. 4–6, under the superficial velocity of liquid of J_L = 0.03 m/s, it is generally seen that, the increase of J_G will increase the pressure gradient and dominant frequency. Meanwhile, to get a more detailed description of the distribution of pressure gradient fluctuations from the PDF, it is necessary to carry out further analysis using the stochastic analysis which includes the pressure gradient average, standard deviation, skewness and kurtosis.

The average pressure gradient obtained from the experiments using three tested liquids of **W**, **G30** and **G50** can be seen in Fig. 7. In the range of J_L and J_G in this study, the increase of both J_L and J_G led to the increase of the pressure gradient. It is in a good agreement with that of Alqoshmal et al. [20]. The increase of liquid viscosity causes also the increase of the pressure gradient. This is caused by the increase of

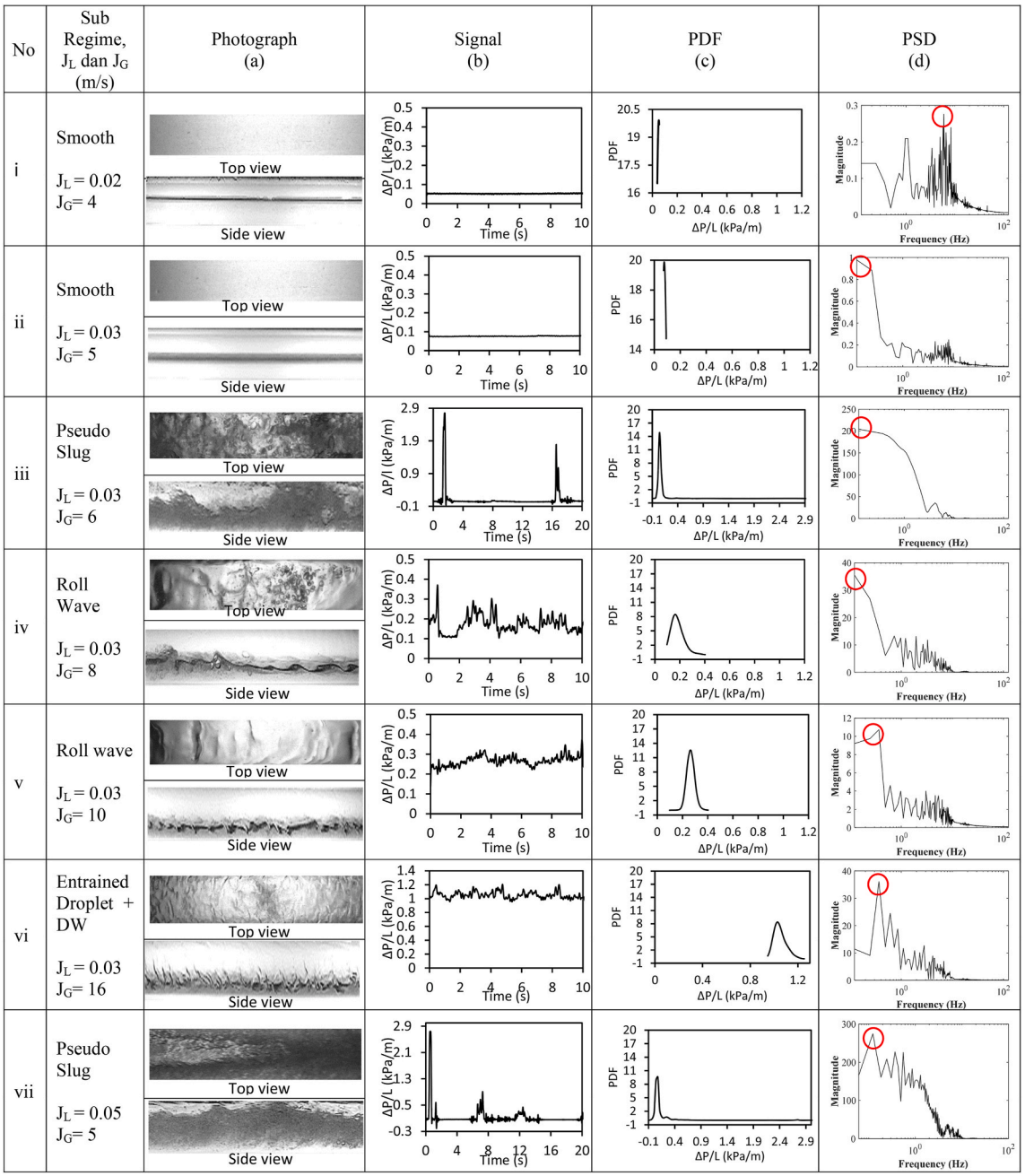

Fig. 6. Example of photos, pressure gradient signal, PDF and PSD of stratified flow regime with liquid fluid (**G50**).

Reynold number (Re_L) will increase the wall shear stress, hence the pressure gradient increases as reported also by Taitel & Dukler [1]. From the three tested liquids, it can be seen that a significant increase in the pressure gradient occurs at $J_G > 12$ m/s, whereas the entrained liquid droplets begin to occur.

The standard deviations of the pressure gradient fluctuations obtained from the experiments using three tested liquids of **W**, **G30** and **G50** are shown in Fig. 8. The figures show that the highest standard deviation occurs in the sub regime of PS, while the lowest occurs in the sub regime of smooth. In the case of **W**, the standard deviation of the pressure gradient of the sub regimes of 2-D and 3-D waves are above the S, but still below the RW, ED + DW and PS. In the sub regime of PS, under a constant of J_L, the increase of J_G causes the decrease of the standard deviation to the lowest position at $J_G = 10$ m/s which indicates the occurrence of RW. The further increase of J_G in the sub regime of RW increases the standard deviation sharply starting from $J_G = 12$ m/s, which indicates the occurrence of ED + DW.

The slope of the pressure gradient distribution can be identified also from the skewness. The measured slope is divided into three curve models (positive, negative and symmetrical) with the reference value of zero (0). The model is positive if the skewness is higher than zero (0) and the curve tail extends to the right. The model is negative if the skewness is less than zero (0) and the curve tail extends to the left. The model is symmetrical if the skewness value is equal to zero (0). Fig. 9 shows the skewness of pressure gradient fluctuations obtained from the experiments. From the three tested liquids, it can be seen that the skewness of the pressure gradient distribution is higher than and equal to zero (0). The skewness of the PS sub-regime is the highest (far above 0) in comparison to that of the other sub-regimes. This indicates that most of the distributions are in low pressure gradient. In the case of the tested liquid of **W**, the sequence of skewness values are PS, RW, ED + DW, 3-D wave, 2-D wave and S sub-regimes. Meanwhile, in the experiments of **G30** and

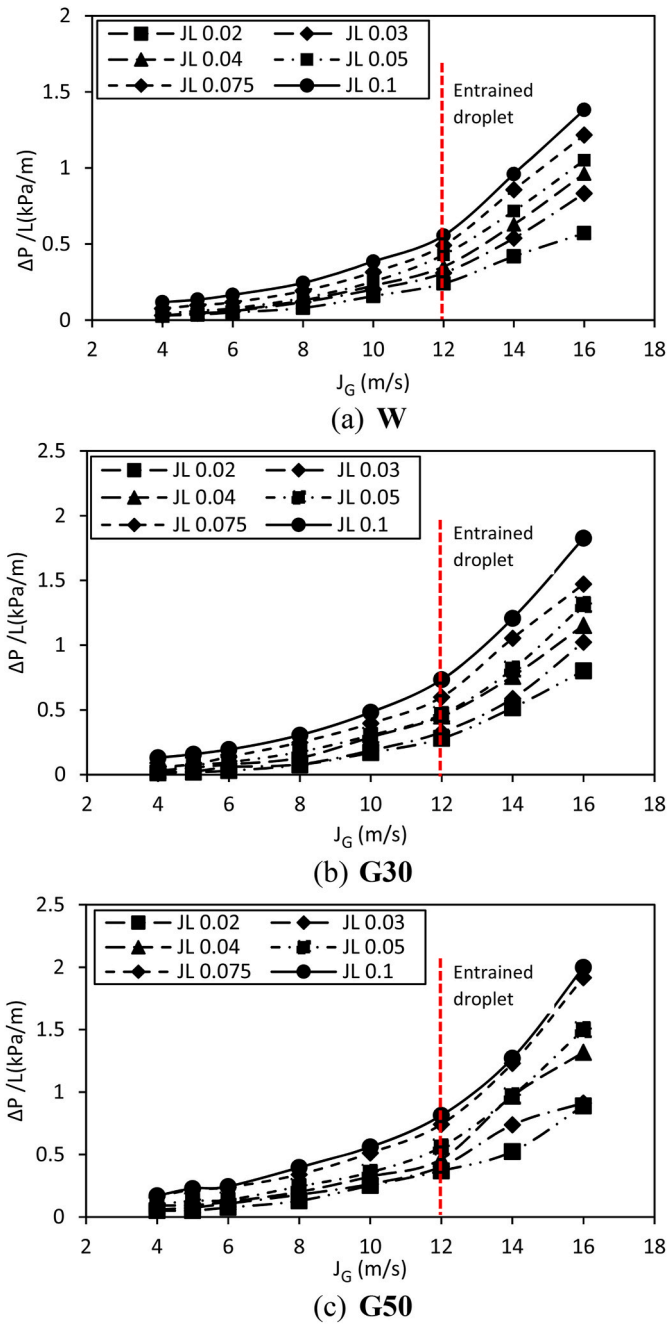

Fig. 7. The effects of both J_L and J_G on the average pressure gradient.

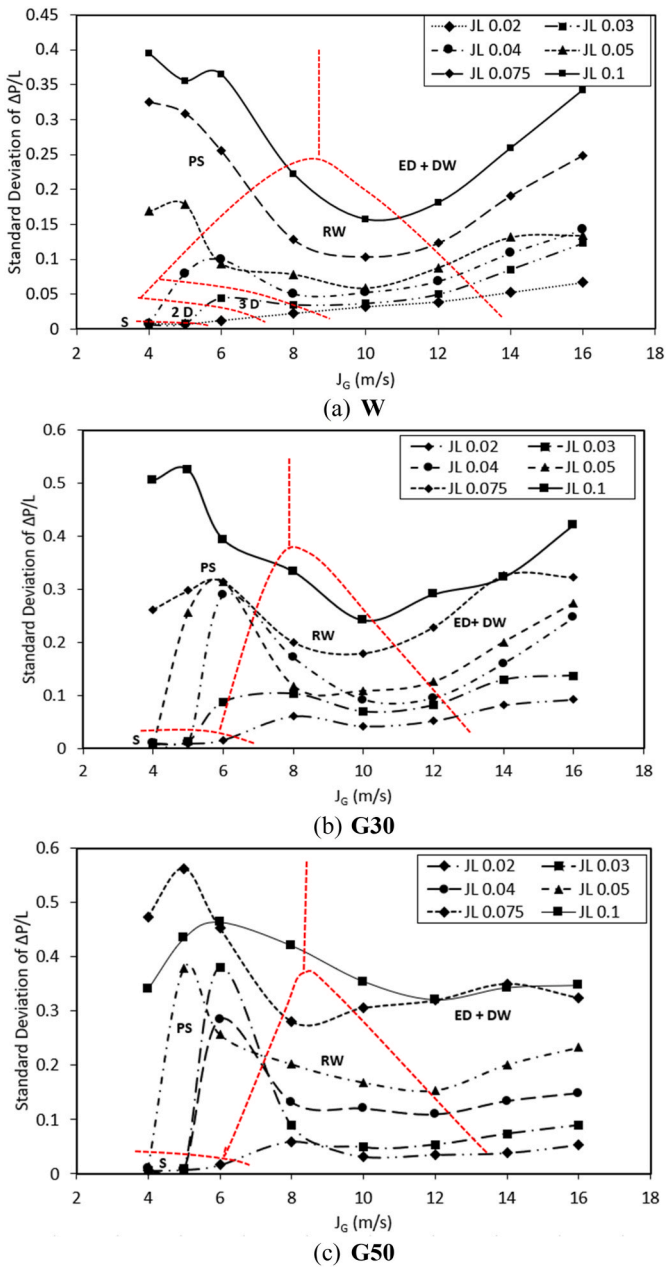

Fig. 8. The effect of both J_L and J_G on the standard deviation of the pressure gradient.

G50, the sequence of skewness values are PS, RW, ED + DW and S sub-regimes. The skewness value in the stratified smooth and 2-D wave sub regimes is ±0, therefore it is noticed that the pressure gradient distribution is normal or symmetrical.

The degree of the sharpness of the pressure gradient distribution in comparison to the normal distribution can be identified from the kurtosis value. Fig. 10 shows the kurtosis of the pressure gradient fluctuations obtained from the experiments of **W**, **G30** and **G50**. From the figure, it is seen that the kurtosis of the pressure gradient distribution in the pseudo slug sub regime is generally higher than 3 (leptokurtic), as can be seen in the PDF which looks very sharp at the low-pressure gradient. This means that most of the pressure gradient fluctuations have almost the uniform low values. Thus, the shape of the PDF with a long tail to the right (very high skewness value) and sharp (very high kurtosis value) is an indication of the pseudo slug sub regime. For the other sub-regimes, it generally has a kurtosis value of less than 3 (platykurtic) as shown in the PDF graph. In the experiment of **W**, the sequence of kurtosis values are PS, RW, 3-D wave, 2-D wave, ED + DW and S sub regimes. In experiments of **G30** and **G50**, the sequence of kurtosis values are the sub-regimes of PS, RW, ED + DW and S.

For comparison, Andritsos [21]; Strand [22] and Ayati & Carneiro [23] have conducted the experiments by using the parallel wire conductance probes and analyzed with kurtosis values to identify wave patterns in the stratified air-water flow. A summary of the experimental conditions of the above works can be seen in Table 3, while the evolution of kurtosis under the increase of J_G from the current experimental data and from the data of previous researchers can be seen in Fig. 11.

Fig. 11 above shows the comparation of the evolution of kurtosis under the increase of J_G from the current experimental data and from the data of previous researchers [Andritsos [21]; Strand [22] and Ayati & Carneiro [23]]. From the figure, it is seen that the results of the

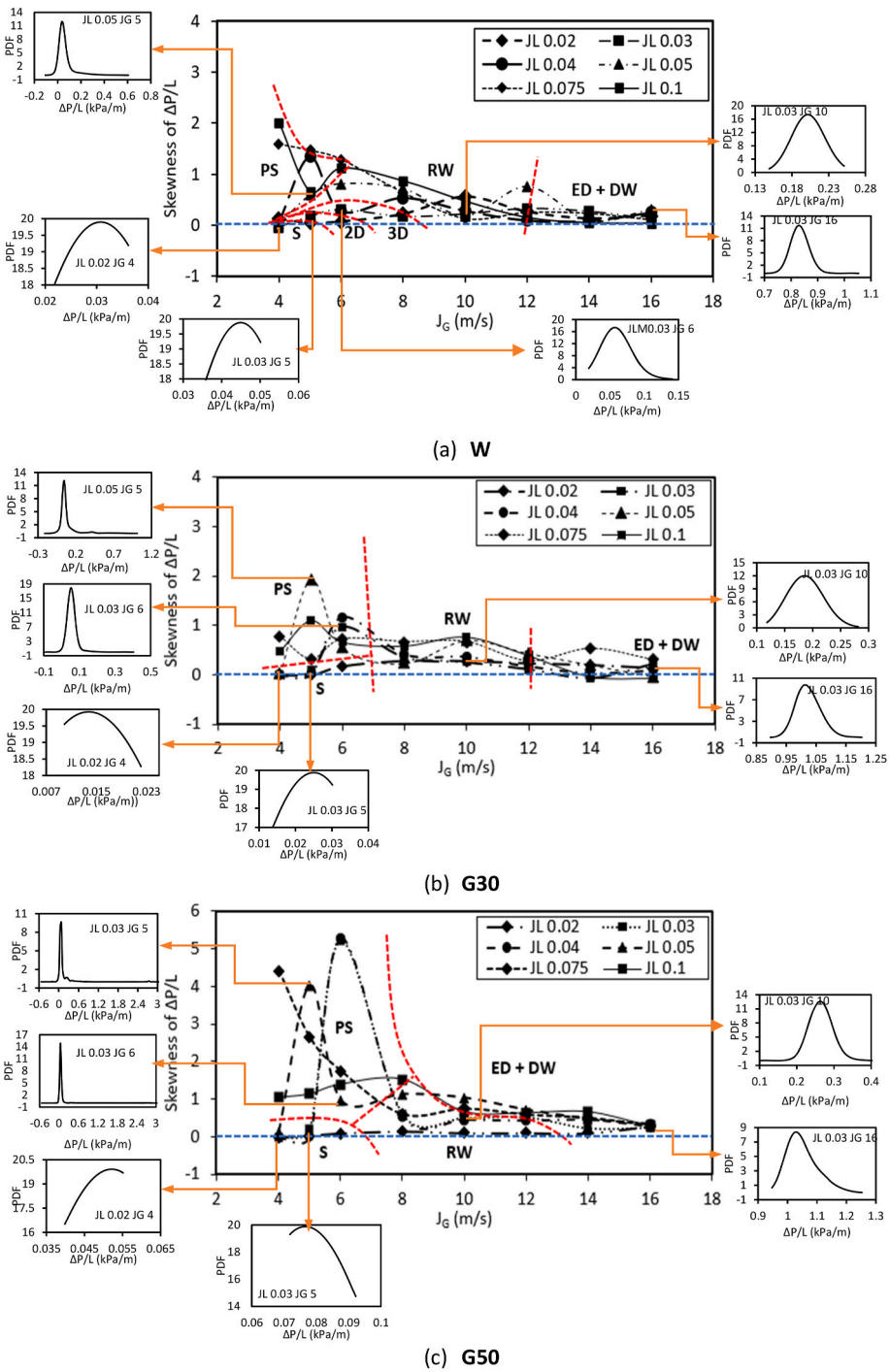

Fig. 9. The effect of both J_L and J_G on the skewness of the pressure gradient.

experiment conducted by Andritsos [21] showed a trend similar to the present study. Andritsos [21] reported that the Pseudo Slug sub-regime occurs at the highest tested liquid viscosity (79 CP), at $J_L = 0.024$ m/s and $J_G = 5$ m/s, which are located in the same PS region for the three tested liquid (**W**, **G30** and **G50**) in the present study. The transition from PS to large amplitude (LA) wave is also the same at $J_G = 6$ m/s. It is generally seen that an increase in J_G decreases the kurtosis which indicates a decrease in wave amplitude. Meanwhile, at $J_G = 6$ m/s to $J_G = 8$ m/s, the increase of liquid viscosity increases the kurtosis which indicates the increase of the wave amplitude. In the present study, ED + DW occurs at $J_G > 12$ m/s, where this is also happened in the experiment of Andritsos [21]; whereas the atomization which is characterized by the presence of droplets touching the upper surface in the pipe.

Although the data of Andritsos [21] and the present study have similar trends and the boundaries of the sub-regimes, there are differences in the kurtosis boundary line. From the above previous data [Andritsos [21]; Strand [22] and Ayati & Carneiro [23]] show that all kurtosis values are positive. They suggest that the kurtosis value of higher than 3 is an indicator of the transition to the large amplitude (LA) wave or roll wave (RW) or also called as the Kelvin Helmhotz (KH) wave. Meanwhile, the value of kurtosis of 3 is wave growth in the form of 2D, the value of kurtosis of 2 is wave stagnation which may be caused by dissipative mechanisms such as air flow separation, wave breaking, interaction of non-linear waves or interaction with bulk flow (both

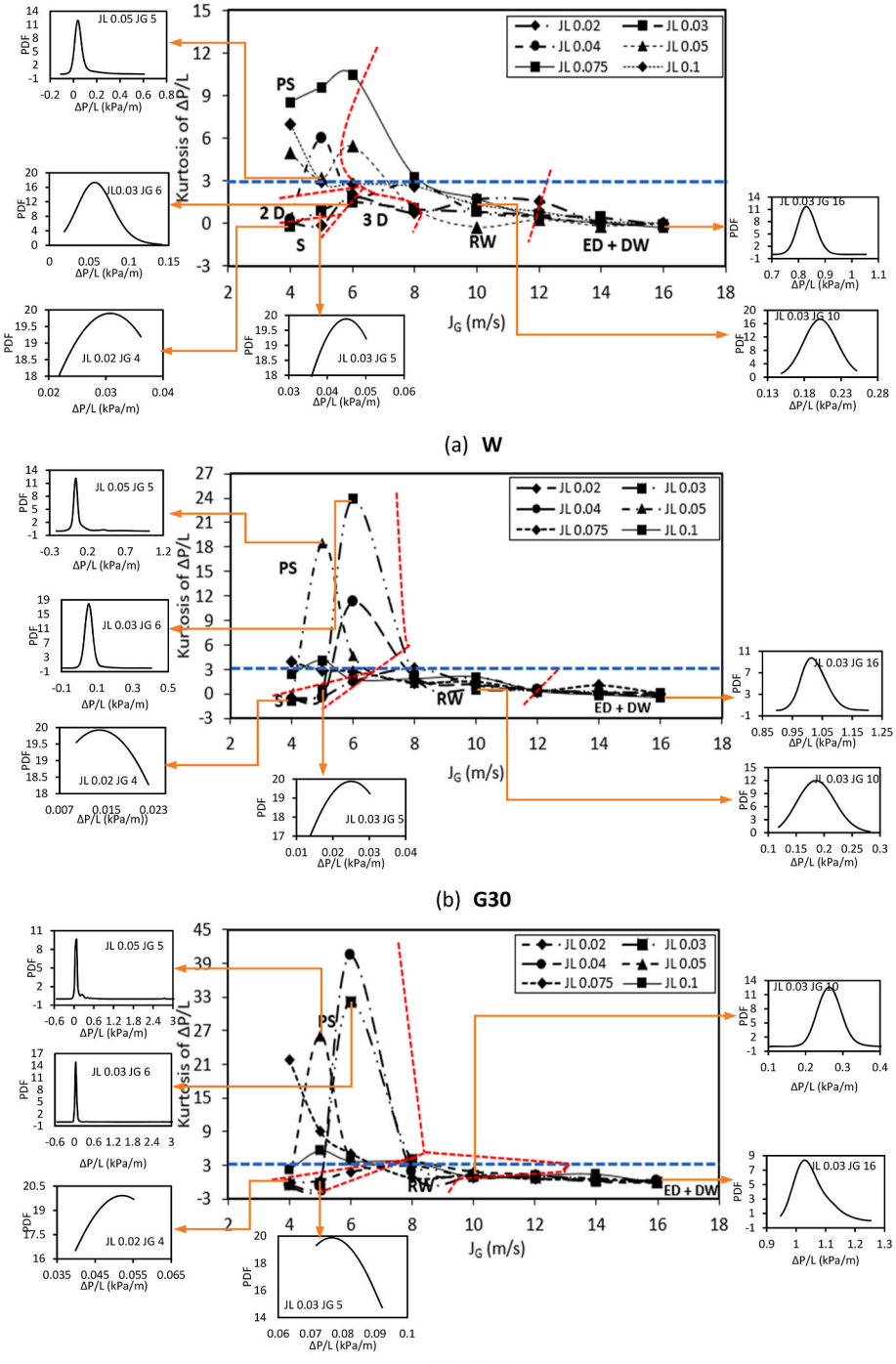

Fig. 10. The effect of both J_L and J_G on the kurtosis of the pressure gradient.

turbulent and sheared). On the other hand, in the experimental present study, a kurtosis value of more than 3 is an indicator of the occurrence of the PS sub regime. In addition, for the sub regimes of 2-D wave, 3-D wave and RW are between 0 and 3, while ED + DW the kurtosis value is 0. The difference in the kurtosis value of the 2-D wave, LA wave and Atomization or ED + DW between the present study and three above previous works might be caused by differences in the characteristics of the sensors used. The three previous researchers used a parallel wire conductance probe, while the present study used a differential pressure transducer (DPT).

From the results of the above three previous studies, this study provides the improvements and has advantages. **First**, by using the limit of $J_G = 4$ m/s to 6 m/s and a kurtosis value of 3, the results of this study are able to provide clear boundaries between the PS sub-regime and other sub-regimes. **Second**, by using the limit of $J_G = 12$ m/s and a negative kurtosis value, this study was able to provide a clearer boundary between the atomization sub-regime or ED + DW with other sub-regimes. **Third**, the use of differential pressure transducer (DPT) is a non-intrusive in comparison to that of the parallel wire conductance probe as used by previous researchers.

3.3. Chaotic analysis

Vial et al. [24] reported that the chaotic systems are characterized by

Table 3
Summary of previous research regarding the identification of interfacial wave patterns in stratified flow by kurtosis analysis.

Researchers (Year)	Work fluids	Experimental Conditions	Measurement Method
Andritsos [21]	1. Gas = Air 2. Liquid: - Water (μ = 1 CP) - Water + 66% glycerine (μ = 16 CP) - Water + 79% glycerine (μ = 70 CP)	1. Pipe length = 10 m, Pipe diameter = 25.2 mm **2. J_G** (6 m/s – 18 m/s) **3. J_L** - Water (μ = 1 CP) (0,01 m/s – 0,06 m/s) - Water + 66% glycerine (μ = 16 CP) (0,002 m/s – 0,02 m/s) - Water + 79% glycerine (μ = 70 CP) (0,002 m/s – 0,02 m/s)	Parallel wire conductance probes consist of a pair of chromel wires (24 A W G) with a diameter of 0.51 mm and a distance between wires of 0.25 mm, placed at a distance of 80D and 160D from the inlet. Sampling rate 1000 Hz
Strand [22]	Air - Water	1. Pipe length = 35 m, Pipe diameter = 100 mm **2. J_G** (0 m/s – 12.5 m/s) **3. J_L** (0.03 m/s – 0.13 m/s)	The parallel wire conductance probes are a pair of gold-plated silver wires, 0.17 mm thick, 4 mm apart and placed 23 m (230D) from the inlet. Sampled rate at 100 Hz for 40.96 s.
Ayati & Carneiro [23]	Air - Water	1. Pipe length = 31 m, Pipe diameter = 100 mm **2. J_G** (1 m/s – 4 m/s) **3. J_L** (0.1 m/s)	Parallel wire conductance probes are a pair of platinum wires with a diameter of 0.3 mm and a distance between wires of 4 mm, placed at a distance of 250D from the pipe inlet. Sample rate 500 Hz

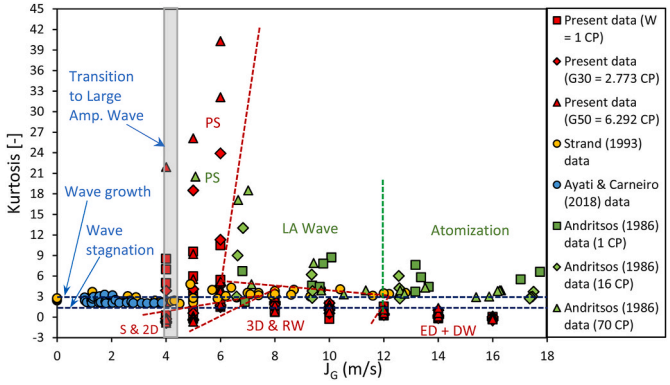

Fig. 11. The effect of J_G on the kurtosis.

the degree of the predictability (small perturbation growth rate) which can be measured by kolmogorov entropy. Fig. 12 shows the effect of both J_L and J_G on the entropy of the fluctuations of the pressure gradient obtained from the present experiments for all the tested liquids. In Fig. 12, (a), (b) and (c) correspond to cases of **W**, **G30**, and **G50** respectively. From the figure, it can be seen that the entropy in the PS sub-regime is the lowest in comparison to the other sub-regimes. This is because most of the pressure gradient fluctuations are almost uniform or homogeneous, while high pressure gradient fluctuations due to hydraulic jumps are very rare. The uniformity of pressure gradient fluctuations at low values of the sub-regime of the PS is shown by high values of both skewness and kurtosis.

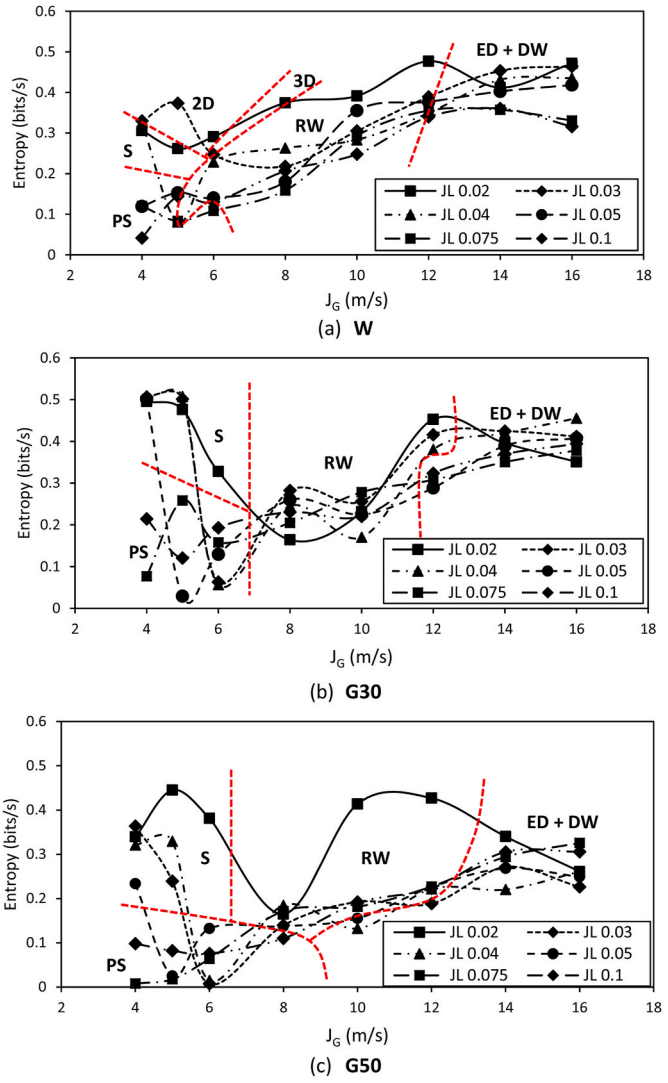

Fig. 12. The effect of the both J_L and J_G on the entropy of the fluctuations of the pressure gradient.

In the sub-regime of stratified smooth (S), although visually it looks flat, in reality there is a small pressure gradient fluctuation which is quite heterogeneous as shown by the low value of kurtosis as discussed above. It makes a higher entropy than PS. The increase of the liquid viscosity causes the entropy in the sub regime of the stratified smooth increases and even partly higher than RW and ED + DW. Meanwhile, in experiments of **W**, the entropy for the sub regime of the 2-D and 3-D are slightly higher than the stratified smooth.

In the sub regime of RW, the increase of J_G will increase the entropy due to the increase of frequency of the disturbance wave, hence the pressure gradient fluctuation becomes more unstable/chaos. The increase of J_G will increase the entropy until the transition of the sub regime of ED + DW, whereas after that the entropy is relatively stable even though the J_G is increased. This is due to the increase of the liquid amount of at the bottom of the pipe that is lifted and turns into entrained droplets, therefore the fluctuations of the pressure gradient become higher. This condition is the beginning of the transition to the annular flow as reported by Lin & Hanratty [2]. In the stratified wavy, it is generally seen from Fig. 12 that the higher the viscosity, the lower the entropy. This means that the increase of the liquid viscosity provides a stabilizing effect to reduce the fluctuations of the pressure gradient.

3.4. Wavelet transform

In the present experimental study, the wavelet transform is used to identify the sub regime in stratified flow from the pressure gradient signals. Wavelet transform decomposes the original signal into a shifted and scaled version. In a decomposed signal, the frequency band decreases with the increase of the signal scale. Here, discrete wavelet transforms (DWT) were implemented to divide the original signal into details, whereas the Daubechies wavelets were used to decompose the signal into ten levels.

Elperin & Klochko [16] clearly determined the maximum decomposition level. Here, the original signal is broken down into ten details. This is considered on the basis of the number of visually identified sub-regimes (6 sub-regimes), hence more detail (levels) is needed to obtain a better identification of sub-regimes from the wavelet transform. Detail one (D1) shows the details of the smallest scale with the highest frequency band, while D2, D3 and so on contain lower frequencies and larger scales as clearly reported by Catrawedarma et al. [25]. The results of the wavelet transform on a sub regime of the stratified flow obtained from the experiments are shown in Figs. 13–15. In column (a) D5 is chosen as an example, taking into account that the position of D5 is in the middle and from the results of the wavelet transform, it is noticed that the highest wavelet energy starts from D5 to D10.

An example of a wavelet energy of a stratified smooth can be seen in column (b) of Figs. 13–15. In general, it can be seen that for the stratified smooth, the highest wavelet energy is at D5, except for $J_L = 0.03$ m/s J_G

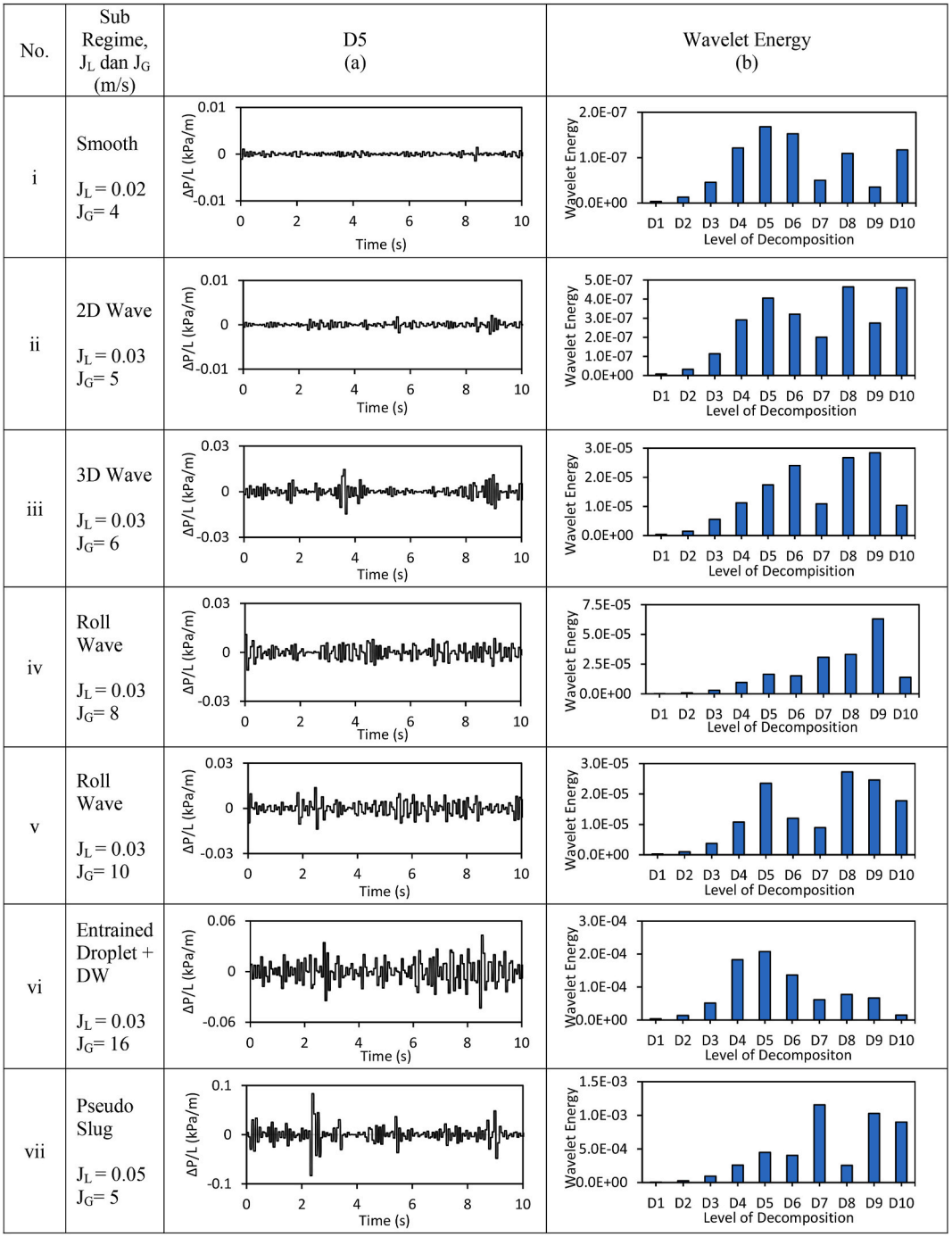

Fig. 13. The wavelet transform results in a stratified flow sub regime (tested liquid of **W**).

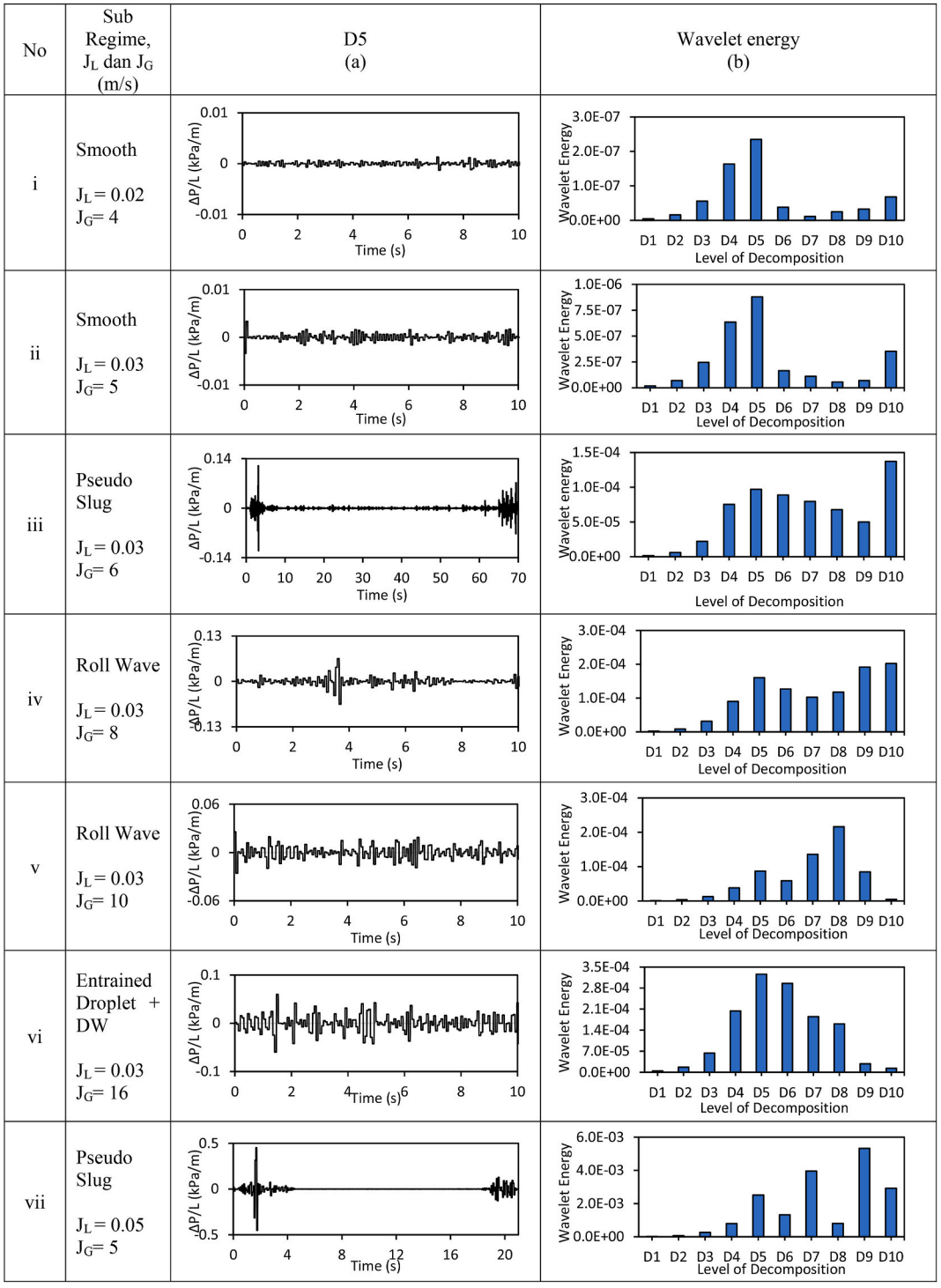

Fig. 14. The wavelet transform results in a stratified flow sub regime (tested liquid of **G30**).

= 5 m/s (fluid **G50**) which is shown in column (b) of Fig. 15 (ii), where D5 and D10 have the same wavelet energy.

From the example of a wavelet energy of **W** – 2-D wave (Fig. 13, ii) or (Fig. 16, ii), it can be seen that the highest wavelet energy is at D8 and the second order is D10. The two decompositions show that the details of the large, low-frequency scale of the pressure gradient fluctuations were caused by the appearance of the clustered 2D. The third order is D5 (medium scale and frequency details) caused by small pressure gradient fluctuations (similar to smooth). The wavelet energy for J_L = 0.02 m/s and J_G = 6 m/s, can be seen in column (b) of Fig. 16 (i). It looks similar to J_L = 0.03 m/s and J_G = 5 m/s, whereas the highest wavelet energy is in D8 and the second order is D10. Meanwhile, under the flow condition of J_L = 0.04 m/s and J_G = 4 m/s, it can be seen in column (b) Fig. 16 (iii), the wavelet energy is different from the previous two pairs of J_L and J_G. The highest energy wavelet is on D6, whereas for a larger scale (D7 to D9) and for a smaller scale (D5 to D1) the wavelet energy is regularly getting lower and D10 is rising again with a height below D8. This is due to the different shape of the 2D wave, whereas the waveform is longer and the occurrence frequency is continuous, not as clustered as in the previous two pairs of J_L and J_G.

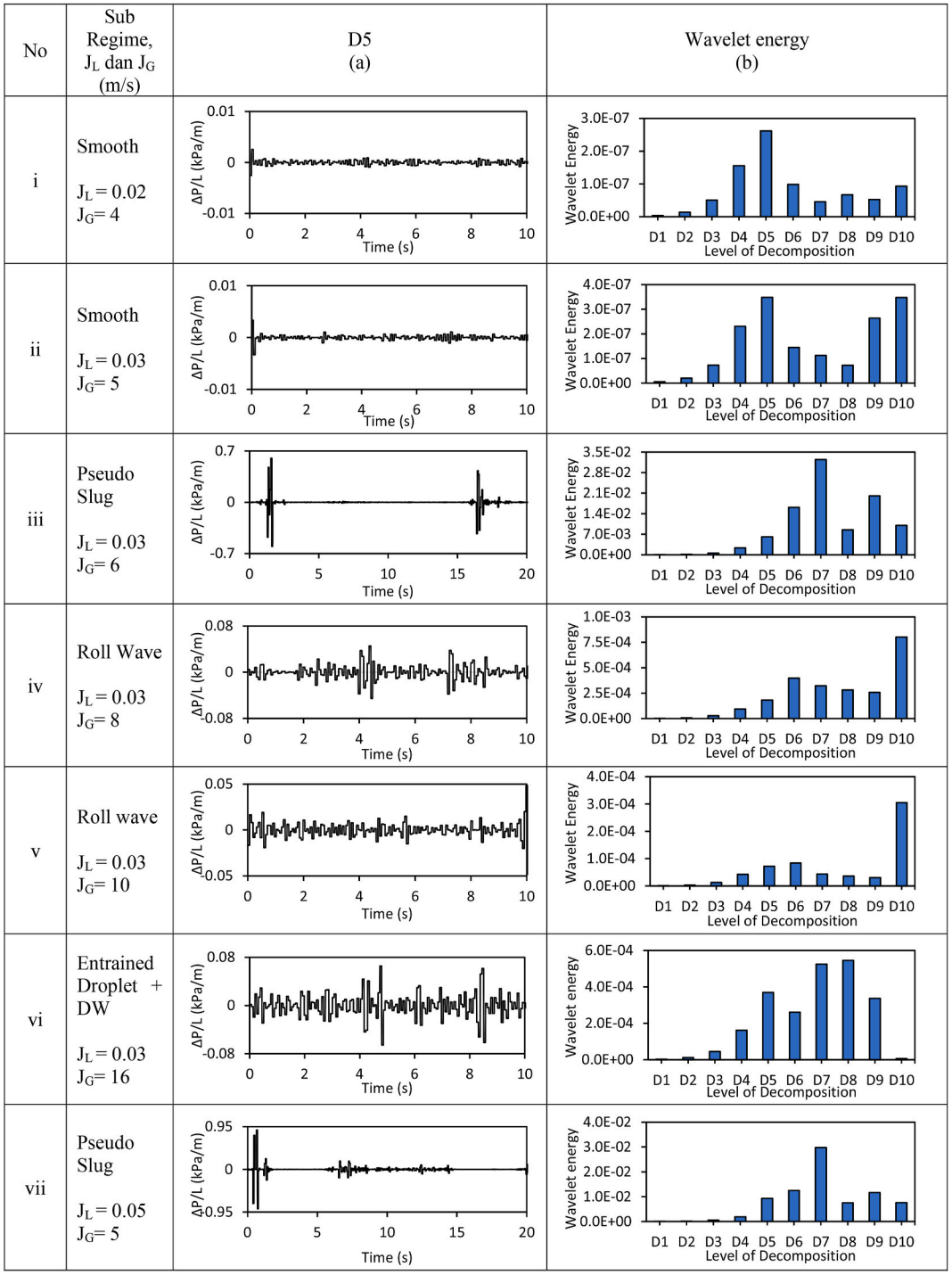

Fig. 15. The wavelet transform results in a stratified flow sub regime (tested liquid of **G50**).

From the example of a wavelet energy of **W** - large 3-D (Fig. 13, iii) or (Fig. 17, ii), it can be seen that the highest wavelet energy is on D9 and D8. Both decompositions show that the large-scale pressure gradient fluctuations with small frequencies is caused by the appearance of quitely infrequent fairly large 3-D waves or with a certain time lag. On a smaller scale of pressure gradient fluctuation with higher frequency, the highest wavelet energy is at D6. It is caused by the small waves (similar to 2-D waves). For **W** - Small 3-D wave (Fig. 17, i), it can be seen that the highest energy wavelet is at D4 and D5. Both decompositions show a high frequency of small pressure gradient fluctuation scale. On the scale of low frequency of large pressure gradient fluctuations, the highest wavelet energy at D9 and D8 is slightly below it.

An example of the wavelet energy of the RW can be seen in column (b) row (iv and v) of Fig. 13 for the tested liquid of **W**, Fig. 14 for **G30** and Fig. 15 for **G50**. For **W** - RW (Fig. 13, iv), it can be seen that the highest wavelet energy in D9 and D8 is slightly below it. Meanwhile, for the lower scale and higher frequencies, the highest wavelet energy is in D5 (with a height which is quite far below D9 and D8). Meanwhile for **W** - RW (Fig. 13, v), with the increase of J_G on the same J_L, it is seen that the highest energy wavelet shifts to D8 and D9. For lower scales and higher frequencies, the highest wavelet energy is at D5 with a height slightly below D8 and D9. This can also be seen from the distribution of pressure

No	J_L and J_G (m/s)	Photograph (a)	Wavelet energy (b)
i	J_L = 0.02 m/s and J_G = 6 m/s		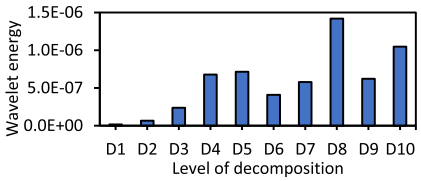
ii	J_L = 0.03 m/s and J_G = 5 m/s		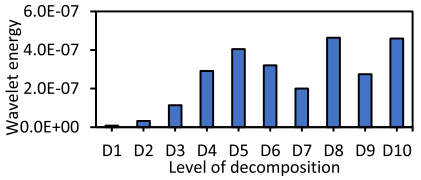
iii	J_L = 0.04 m/s and J_G = 4 m/s		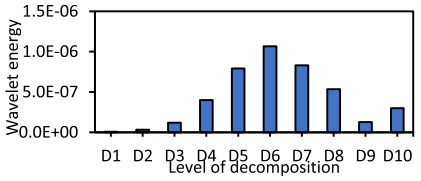

Fig. 16. Photograph and wavelet energy for the 2-D wave sub regime.

No	J_L dan J_G (m/s)	Photograph (a)	Wavelet energy (b)
i	J_L = 0.02 m/s and J_G = 8 m/s		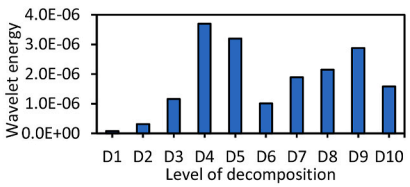
ii	J_L = 0.03 m/s and J_G = 6 m/s	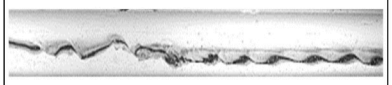	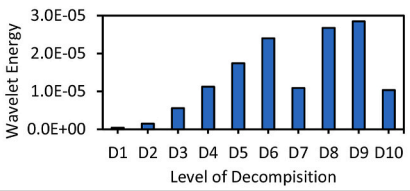

Fig. 17. Photograph and wavelet energy for the 3-D wave sub regime.

gradient fluctuations in the skewness in Fig. 9 (a) which looks symmetrical (close to 0) and the kurtosis in Fig. 10 (a) which looks sloping (<3).

For **G30** – RW (Fig. 14, iv), it can be seen that the highest wavelet energy is in D10 (D9 is almost the same slightly below D10). For lower scales and higher frequencies, the highest wavelet energy is at D5 with a height slightly below D9 and D10. This shows that the large and small-scale wavelet energies are almost the same. This can also be seen from the distribution of pressure gradient fluctuations in the skewness in Fig. 9 (b) which looks slightly above zero and the kurtosis in Fig. 10 (b) which looks close to normal (almost equal to 3). J_L = 0.03 m/s and J_G = 10 m/s as shown in column (b) of Fig. 14 (v), it is noticed that the increase of J_G, it is seen that the highest energy wavelet shifts to D8 (D7 is slightly below it). For lower scales and higher frequencies, the highest wavelet energy is at D5 with a height far below D7 and D8. For **G50** – RW (Fig. 15, iv), it can be seen that the highest wavelet energy is at D10 (much higher value than other decomposition levels). For lower scales and higher frequencies, the highest wavelet energy is at D6. Meanwhile for **G50** – RW (Fig. 15, v), it is noticed that the increase of J_G, the highest wavelet energy is still the same at D10. For lower scales and higher frequencies, the highest energy wavelets are still the same at D6, where from D6 sequentially decreases to decomposition levels with smaller scales D5 and D4. From the wavelet analysis in the RW sub regime, it shows that the increase of the liquid viscosity shifts the wavelet energy to a larger scale and lower frequency. In addition, the increase of J_G will increase the wavelet energy at the small-scale and high-frequency decomposition levels.

An example of a wavelet energy of the sub regime of ED + DW under the flow condition of J_L = 0.03 m/s and J_G = 16 m/s can be seen in column (b) row (vi) of Fig. 13 for **W**, Fig. 14 for **G30** and Fig. 15 for **G50**. In the experiment of **W**, it is seen that the highest wavelet energy is at D5. Meanwhile, for large scale and lower frequencies, the highest wavelet energy is in D8 with its height far below D5. In the experiment of **G30**, it is seen that the highest wavelet energy is at D5. In the experiment of **G50**, it is seen that the highest wavelet energy is at D8. Meanwhile, for small scale and higher frequencies, the highest wavelet energy is in D5. From the wavelet analysis in the sub-regime of ED + DW, it is noticed that the increase of liquid viscosity shifts the wavelet

energy to a larger scale and lower frequency.

From the wavelet analysis above, it is shown that the increase of the J_G under a constant of J_L causes an increase in wavelet energy at small-scale and high-frequency decomposition rates. This is due to the increasing relative velocity or slip between the gas and liquid phases, hence the frequency of the interfacial wave formation increases. This causes the increase of frequency of pressure gradient fluctuations. However, the increase of J_G causes the interfacial waves to be pushed forward, hence the formation of large wave amplitudes could not possible. It makes the decrease of the amplitude of the waves, and the scale of the pressure gradient fluctuations is become smaller. Moreover, the increase of the liquid viscosity causes the wavelet energy to shift to a larger scale and a lower frequency. This is due to the need for higher forces to form interfacial waves with higher liquid viscosity. Hence, under the same J_G and J_L, the increase in the viscosity of the liquid causes the wave frequency to decrease. This causes the frequency of pressure gradient fluctuations to be lower, but the scale increases due to the increase of the friction factor.

An example of the wavelet energy of the PS under the flow condition of $J_L = 0.05$ m/s and $J_G = 5$ m/s can be seen in column (b) row (vii) of Fig. 13 for **W**. Meanwhile for $J_L = 0.03$ m/s and $J_G = 6$ m/s, it can be seen in column (b) row (iii) Fig. 14 for **G30** and Fig. 15 for **G50**. From the experiments of the tested liquid of **W** it is noticed that the highest wavelet energy is at D7. From the experiments of **G30**, it shows that the highest wavelet energy at D9. From the experiments of **G50**, it shows that the highest wavelet energy is at D7. Meanwhile, for **G30 -** PS (Fig. 14, iii), it shows that the highest wavelet energy is at D10. For **G50 –** PS (Fig. 15, iii) it shows that the highest wavelet energy at D7. From the above facts, it can be seen that the increase of the liquid viscosity, the wavelet energy of the pseudo slug sub regime also increases, but the wavelet energy shifts to a smaller scale with a higher frequency.

In comparison to the results of the analysis of the three methods (PDF, PSD, Kolmogorov entropy), Discrete Wavelet Transform (DWT) is able to better identify the stratified flow sub-regime based on the wavelet energy and decomposition level. The results of identification using the PDF, PSD and Kolmogorov entropy methods can be used to strengthen the identification results of DWT.

4. Conclusions

The interfacial behavior of the sub-regimes of the gas-liquid stratified two-phase flow was identified visually and using differential pressure signal data. In the present experiment, the working fluid were air and water with three variations of viscosity. Those are water (**W**), water + 30% glycerine (**G30**) and water + 50% glycerine (**G50**). Here, probability distribution function (PDF), power spectral density (PSD), kolmogorov entropy and discrete wavelet transform (DWT) were used to analyze the differential pressure signal. The quantification of the PDF was accomplished using the average, standard deviation, skewness and kurtosis. The results are summarized as follows:

a. There are six identified sub-regimes of the stratified flow. Those are stratified smooth (S), two-dimensional (2-D) wave, three-dimensional (3-D) wave, roll wave (RW), entrained droplet and disturbance wave (ED + DW) and pseudo slug (PS). The increase of the liquid viscosity causes the transition line from the RW to ED + DW shifts to a lower both J_L and J_G.
b. A significant increase of the pressure gradient occurs at $J_G > 12$ m/s, where the entrained liquid droplets begin to occur. The increase of the liquid viscosity causes the increase of the pressure gradient.
c. The entropy in the PS sub-regime is the lowest in comparison to that of the other sub-regimes. This is because the pressure gradient fluctuations are almost uniform without any hydraulic jump. In the sub-regime of S, there is a small pressure gradient fluctuation which is quite heterogeneous. It makes a higher entropy than PS. For the sub-regimes of both the 2-D and 3-D waves are slightly higher than the S. In the sub regime of RW, the increase of J_G will increase the entropy which is caused by the increase of the frequency of the disturbance wave, hence the pressure gradient fluctuation becomes more unstable/chaos. The increase of J_G causes the continue increases of the entropy until near the transition of the sub regime of ED + DW, whereas after that the entropy is relatively stable even though the J_G is increased.
d. In the sub regime of RW, the increase of the liquid viscosity shifts the wavelet energy to a larger scale and lower frequency. Next, the increase of J_G causes an increase in wavelet energy at the smaller-scale and higher-frequency decomposition levels, namely from the initial condition the highest wavelet energy at D9 shifts to D8 for **W** and from D10 shifts to D8 for **G30**. Meanwhile for liquid tested of **G50**, the increase of J_G, the highest wavelet energy is still the same at D10.
e. In the sub regime of ED + DW, the increase of the liquid viscosity shifts the highest wavelet energy to shift to a larger scale and lower frequency, namely D5 for liquid tested of **W** and **G30**, and D8 for **G50.** For the sub regime of PS, the increase of the liquid viscosity will increase the wavelet energy of the pseudo slug sub regime, but the wavelet energy shifts to a smaller scale with a higher frequency.

Author statement

Setya Wijayanta: Experimental data investigation, Design of the experimental facility, Drafting manuscript, Revised manuscript, acquisition of data, analysis/interpretation of data, Approval of the version of the manuscript to be published, **Indarto:** Research funding, Supervision, Approval of the version of the manuscript to be published, **Deendarlianto:** Conception and design of study, revising the manuscript critically for important intellectual content, Supervision, Research funding, Approval of the version of the manuscript to be published, **IGNB. Catrawedarma:** Experimental data investigation, analysis/interpretation of data, Approval of the version of the manuscript to be published, **Akhmad Zidni Hudaya:** Manufacture of the facility, Acquisition of data, Analysis/interpretation of data, Approval of the version of the manuscript to be published.

Declaration of competing interest

The authors declare that they have no known competing financial interests or personal relationships that could have appeared to influence the work reported in this paper.

Acknowledgments

The current study was conducted within the framework of an ongoing research project at the Multiphase Flow Research Group, Fluid Mechanics Laboratory, Universitas Gadjah Mada, Indonesia. The author would like to thank Dr. Eko Prasetya Budiana, Achilleus Hermawan Astyanto, Haslinda Kusumaningsih, for the discussion and Ari Prasetya, Chistoforus Yacob S. and Prakoso who have supported the manufacturing of the apparatus. Setya Wijayanta acknowledge the Indonesia Endowment Fund for Education/Lembaga Pengelola Dana Pendidikan (LPDP), the Ministry of Finance of the Republic of Indonesia for funding support through Doctoral Scholarships and Research Funding Assistance and the Ministry of Transportation of the Republic of Indonesia for providing support in continuing Doctoral Education.

References

[1] Y. Taitel, A.E. Dukler, A model for predicting flow regime transitions in horizontal and near horizontal gas-liquid flow, AIChE J. 22 (1) (1976) 47–55.
[2] P.Y. Lin, T.J. Hanratty, Prediction of the initiation of slugs with linear stability theory, Int. J. Multiphas. Flow 12 (1) (1986) 79–98.
[3] J.T. Hanratty, A. Hershman, Initiation of roll waves, AIChE J. 7 (9) (1961) 488–497.

[4] Kenneth Bruno, A Study of Interfacial Waves in Gas-Liquid Flows, Disertation. Department of Chemical Engineering, Notre Dame, Indiana, 1988.
[5] O. Dinaryanto, A. Widyatama, A.I. Majid, Indarto Deendarlianto, Image processing analysis on the air-water slug two-phase flow in a horizontal pipe, AIP Conf. Proc. 1737 (2016).
[6] O. Dinaryanto, Y.A.K. Prayitno, A.I. Majid, A.Z. Hudaya, Y.A. Nusirwan, A. Widyaparaga, Deendarlianto Indarto, Experimental investigation on the initiation and flow development of gas-liquid slug two-phase flow in a horizontal pipe, Exp. Therm. Fluid Sci. 81 (2017) 93–108.
[7] R.E. Vieira, N.R. Kesana, C.F. Torres, B.S. McLaury, S.A. Shirazi, E. Schleicher, U. Hampel, Experimental investigation of horizontal gas-liquid stratified and annular flow using wire-mesh sensor, J. Fluid. Eng. Trans. ASME 136 (12) (2014).
[8] G.W. Govier, M.M. Omer, The horizontal pipeline flow of air-water mixtures, Can. J. Chem. Eng. 40 (3) (1962) 93–104.
[9] Mandhane, A flow pattern map for gas-liquid in horizontal piper, Int. J. Multiphas. Flow 1 (1974) 537–553.
[10] P.L. Spedding, V.T. Nguyen, Regime maps for air water two phase flow, Chem. Eng. Sci. 35 (4) (1980) 779–793.
[11] X.T. Chen, X.D. Cai, J.P. Brill, Gas-liquid stratified-wavy flow in ihorizontal pipelines, J. Energy Resour. Technol., Trans. ASME 119 (4) (1997) 209–216.
[12] M. Fernandino, T. Ytrehus, Determination of flow sub-regimes in stratified air-water channel flow using LDV spectra, Int. J. Multiphas. Flow 32 (4) (2006) 436–446.
[13] A.Z. Hudaya, A. Widyatama, O. Dinaryanto, W.E. Juwana, Deendarlianto Indarto, The liquid wave characteristics during the transportation of air-water stratified co-current two-phase flow in a horizontal pipe, Exp. Therm. Fluid Sci. 103 (July 2018) (2019) 304–317.
[14] N. Andritsos, L. Williams, T.J. Hanratty, Effect of liquid viscosity on the stratified-slug transition in horizontal pipe flow, Int. J. Multiphas. Flow 15 (6) (1989) 877–892.
[15] H. Matsubara, K. Naito, Effect of liquid viscosity on flow patterns of gas-liquid two-phase flow in a horizontal pipe, Int. J. Multiphas. Flow 37 (10) (2011) 1277–1281.
[16] T. Elperin, M. Klochko, Flow regime identification in a two-phase flow using wavelet transform, Exp. Fluid 32 (11) (2002) 674–682.
[17] S.G. Mallat, Multiresolution approximations and wavelet orthonomal bases of L^2(R), Trans. Am. Math. Soc. 315 (9) (1989) 69–87.
[18] B. Bae, T. Ahn, J. Jeong, K. Kim, B. Yun, Characteristics of an interfacial wave in a horizontal air-water stratified flow, Int. J. Multiphas. Flow 97 (2017) 197–205.
[19] A.E. Dukler, M.G. Hubbard, A model for gas-liquid slug flow in horizontal and near horizontal tubes, Ind. Eng. Chem. Fundam. 14 (1975) 337–346, 4 (6).
[20] Y.M. Alqoshmal, A.Z. Hudaya, O. Dinaryanto, A. Widyatama, Deendarlianto & Indarto, The characteristics of the pressure gradient air-water stratified two-phase flow in horizontal pipes, AIP Conf. Proc. 30003 (2018). No. 1. AIP Publishing.
[21] Nikolaos Andritsos, Effect of Pipe Diameter and Liquid Viscosity on Horizontal Stratitifed Flow, Phd thesis, Univ. Illinois, Urbana, 1986.
[22] O. Strand, An Experimental Investigation of Stratified Two-phase Flow in Horizontal Pipes, PhD thesis, University of Oslo, 1993.
[23] A.A. Ayati, J.N.E. Carneiro, Statistical characterization of interfacial waves in turbulent stratified gas-liquid pipe flows, Int. J. Multiphas. Flow 103 (2018) 94–105.
[24] C. Vial, E. Camarasa, S. Poncin, G. Wild, N. Midoux, J. Bouillard, Study of hydrodynamic behaviour in bubble columns and external loop airlift reactors through analysis of pressure fluctuations, Chem. Eng. Sci. 55 (2000) 2957–2973.
[25] I.G.N.B. Catrawedarma, Indarto Deendarlianto, Statistical characterization of flow structure of air-water two-phase flow in airlift pump-bubble generator system, Int. J. Multiphas. Flow 138 (2) (2021) 1–16.
[26] S. Cai, T. Haluk, Q. Jianhung, S.A. John, Neural network based objective flow regime identification in air-water two phase flow, Can. J. Chem. Eng. 72 (1994) 440–445.
[27] J. Drahos, J. Tihon, C. Serio, A. Liibbert, Deterministic chaos analysis of pressure fluctuations in a horizontal pipe at intermittent flow regime, Chem. Eng. J. 64 (1996) 149–156.
[28] H. Wu, F. Zhou, Y. Wu, Intelligent identification system of flow regime of oil-gas-water multiphase flow, Int. J. Multiphas. Flow 27 (3) (2001) 459–475.
[29] B. Santoso, Deendarlianto Indarto, S.W. Thomas, The identification of gas-liquid co-current two-phase flow pattern in a horizontal pipe using the power spectral density and the artificial neural network (ANN), Mod. Appl. Sci. 6 (8) (2012) 56–67.
[30] S. Saini, J. Banerjee, Recurrence analysis of pressure signals for identification of intermittent flow sub-regimes, J. Petrol. Sci. Eng. 204 (4) (2021) 1–15.
[31] S. Saini, J. Banerjee, Recognition of onset of slug using recurrence analysis of pressure signal, Nucl. Eng. Des. 381 (6) (2021) 1–12.